quaternary

MDPI

Article

Revisit the Medieval Warm Period and Little Ice Age in Proxy Records from Zemu Glacier Sediments, Eastern Himalaya: Vegetation and Climate Reconstruction

Nivedita Mehrotra [1], Nathani Basavaiah [2] and Santosh K. Shah [1,*]

[1] Birbal Sahni Institute of Palaeosciences, 53 University Road, Lucknow 226007, India
[2] Indian Institute of Geomagnetism, Navi Mumbai 410206, India
* Correspondence: santoshkumar_shah@bsip.res.in or santoshk.shah@gmail.com

Abstract: The Late Holocene fossil pollen records from the Zemu glacier, located in Yabuk, North Sikkim, in the eastern Himalayas, effectively generated quantitative climate reconstructions based on the transfer function model. The transfer function model was developed by establishing a modern pollen–climate calibration set from the temperate alpine belt of North Sikkim. A redundancy analysis was carried out to detect the pattern of variation of climatic variables in the modern pollen datasets. The mean annual precipitation (MAP) and mean temperature of the warming month (MTWA) had the strongest influence on the composition of the modern pollen samples among the climatic variables considered in the analysis. Proxy data in the form of fossil pollen records were analyzed for reconstructing past climate based upon the relationships between modern pollen vegetation assemblages and climatic patterns. Transfer functions for MAP and MTWA were developed with the partial least squares (PLS) approach, and model performance was assessed using leave-one-out cross-validation. The validated model was used to reconstruct MAP and MTWA for the last 2992 cal years BP (1042 BC) in North Sikkim. The variability observed in the reconstructions was analyzed for past global climatic events. It was further compared with the available regional and hemispheric proxy-based climate reconstructions. The reconstructions captured comparable Medieval Warm Period (MWP) and Little Ice Age (LIA)-like events from the Zemu glacier region. The fossil pollen data and climate reconstructions were further compared with the mineral magnetism data of the subsurface sediment profile.

Keywords: Late Holocene; pollen; mineral magnetism; transfer function; PLS; MAP; MTWA

Citation: Mehrotra, N.; Basavaiah, N.; Shah, S.K. Revisit the Medieval Warm Period and Little Ice Age in Proxy Records from Zemu Glacier Sediments, Eastern Himalaya: Vegetation and Climate Reconstruction. *Quaternary* **2023**, *6*, 32. https://doi.org/10.3390/quat6020032

Academic Editor: Elda Russo Ermolli

Received: 31 December 2022
Revised: 21 April 2023
Accepted: 5 May 2023
Published: 9 May 2023

1. Introduction

The decadal-to-millennial-scale climate variability records of the Quaternary period are of significant interest to scientists; their chronology and mechanisms have been widely discussed, prompting extensive analysis and recommendations [1]. However, further detailed analysis is needed in order to obtain a deeper understanding of the authenticity of past climate change studies. An introspective look at the dynamics and functioning of the past climatic system will allow us to understand its behavior and patterns in the future. This will improve greatly if long-term climate data are available beyond the existing instrumental records. Thus, palaeoclimatic data are essential to obtain comprehensive information about the past climate system, without which reliable forecasting of future conditions will not be possible [2]. High-elevation mountainous regions also represent unique areas for the detection of climatic change and the assessment of climate-related impacts [3]. One reason for this is that, as the climate changes rapidly with altitude over relatively short horizontal distances, so do vegetation and hydrology [4]. Past climate records from such high-elevation mountainous regions and remote areas can be used to evaluate the regional climate and its association with global climate dynamics. These high-altitude environments comprise glaciers, snow, permafrost, water, and the uppermost

limits of vegetation and other complex life forms in the mountains, and they are the most sensitive to climatic changes occurring on a global scale [5].

Instrumental meteorological records from high-altitude sectors of the Himalayas, such as regions in proximity to glaciers, do not cover a longer time span as they were not recorded before the last century. Thus, assessing long-term climatic variability in higher elevations and remote regions of the Himalayas as well as its future impact is hindered by the paucity of long-term meteorological and glaciological observations. For this, extensive climate records from natural archives and proxies are required. Based on these natural archives or proxy data, detailed climate reconstructions have been carried out globally [6,7]. Proxy-based climate reconstructions can be useful to place recent climate trends in the context of a longer time scale. These climate reconstructions allow a comparison to be made of recent trends with past climatic variation and with well-known climatic events of the Late Holocene period, such as the Medieval Warm Period (MWA), or Epoch (MWE) [8], more recently coined as the Medieval Climatic Anomaly (MCA) [9–11], and the Little Ice Age (LIA) [12]. It also facilitates assessing the local pattern of climate variability in a regional, continental, hemispheric, and global context. The quantitative climate reconstructions from the Himalaya region are mostly available from tree-ring proxy records [13] and are highly concentrated in the western Himalayan region [13]. Only a few tree-ring-based temperature reconstructions are available from the eastern Himalayas, including parts of India [14,15] and Bhutan [16]. Tree-ring data were used by Bhattacharyya and Chaudhary [14] for temperature reconstruction from the eastern Himalayan region carried out in sites close to the present pollen study sites.

The pollen grains preserved in sub-surface sediments have been extensively studied as a proxy indicator of palaeoclimatic and palaeoecological changes during the Quaternary period [7,17], and many methodological advances in various fields have been made during the last five decades [18–22]. Palynological analysis of the Quaternary sediment from temperate to alpine regions of the Himalayas has been carried out for past vegetation vis-à-vis climate analysis [23,24]. These records mainly show qualitative past climate based on the vegetation assemblages during the Late Quaternary. However, quantitative past climate reconstruction using the pollen dataset is poorly studied in the Indian Himalayan region and absent from Sikkim in the eastern Himalayas [25]. In spite of the fact that quantitative climate reconstruction of temperature and precipitation based on modern pollen–climate relationships are useful for perceiving Quaternary Palaeoecology and Palaeoclimatology [26], various climatic variables such as mean annual temperature (MAT), mean temperature of the coldest month (MTCO), mean temperature of the warmest month (MTWA), and mean annual precipitation (MAP) are widely experimented climatic parameters. These have been applied in several quantitative climatic reconstructions using a variety of proxies. After the pioneering works of Iverson [27] and Grichuk [28], pollen data from lacustrine and sedimentary archives became the most frequently used proxy to quantify changes in the Holocene and Pleistocene climate from various geographical regions [29]. The algorithm for the reconstruction of environmental variables using biological proxies was introduced long ago by Imbrie and Kipp [30]. Since then, pollen climate transfer functions have been widely attempted for the quantitative reconstruction of climatic parameters on different geological time scales from various parts of the globe [31–52]. Pollen-based quantitative climate reconstruction has made great strides over the past few decades in various parts of the world, using several different reconstruction techniques [53]. Transfer function-based climate reconstruction using pollen records has also made advances in Asian subcontinents [54–66].

The strengths and weaknesses of quantitative climate reconstruction using pollen as a proxy, modeled with discrete transfer function methods as demonstrated in the reviews [17,20,26,37,38,67–76], are discussed by Birks [77]. However, these widely studied climate reconstruction techniques have not been widely applied in the eastern Himalayan region despite the availability of the pollen-based Late Quaternary records [25]. There are few studies in which the coexistence approach has been used to reconstruct quantitative

climate during the Late Quaternary period using pollen [78] and phytolith [79] records from the eastern Himalayas. The coexistence approach was introduced by Mosbrugger and Utescher [80] for the quantitative reconstruction of Tertiary terrestrial palaeoclimates using plant fossils. It is not widely used for fossil pollen-based climate reconstruction, especially for the Holocene. The limited take-up of the coexistence approach in Holocene studies is because other related methods, such as direct transfer functions, are available [81]. However, this technique has been used in China for several Holocene pollen records [82,83].

The fossil pollen studies previously carried out in Sikkim have mostly deduced past vegetation with qualitative reconstructions of the climate. Late Holocene vegetation climate history was reported based on fossil records from Khechipiri Lake [84] and Kupup Lake [85] located in Sikkim, the Himalayas. In the adjoining temperate parts of this region, few fossils pollen studies have been carried out [86,87]. Sharma and Chauhan [86] have reported vegetation history dating from the Last Glacial Maximum (LGM) based on pollen records from Mirik Lake, Darjeeling Himalaya. Other studies from Jore-Pokhari, a temperate lake located in Darjeeling Himalaya [87], described qualitative climatic records since 2500 cal. BP. In addition, there is no modern pollen climate calibration set that is a pre-requisite for quantitative climate reconstruction. The surface pollen spectra from Sikkim Himalaya have been studied at only one site [85]. The study included the relationship between vegetation and modern pollen rain from the Kupup Lake vicinity using 12 surface samples, but no quantitative comparisons with the modern climate of the region have yet been established. Similarly, there is one recent study of only modern pollen data sets from the North Sikkim region, and emphases have been placed on the feasibility of the data for future palaeovegetation and palaeoclimatic reconstruction [88]. However, in this study, no pollen fossil data sets were utilized for palaeoclimate reconstruction. Thus, the development of pollen-based quantitative climate reconstruction using the transfer function model in the eastern Himalayas is needed.

Here, we make the first attempt to reconstruct climate in quantitative terms and to assess its past variation at the Zemu glacier, eastern Himalaya. We try to establish the possible roles of regional climate, global teleconnection, and long-term climate variation in the Zemu glacier, eastern Himalaya. In this study, modern pollen climate calibration was established and applied to a Late Holocene fossil pollen record from Yabuk, Zemu glacier, North Sikkim, for quantitative past climate reconstruction. The reconstructed climatic variables were further compared to the environmental geomagnetic data of the profile sediments. The study of the mineral magnetic properties of sediments has become an increasingly useful tool to understand the input of sediment flux in different depositional environments containing iron mineral particles [89–93]. The technique is useful for reconstructing climate and environment because the mineral magnetic characteristics of sediments are sensitive to variations in climate, transport medium, and environmental conditions [90,91,94–96]. Lake sediment properties of magnetic susceptibility and remanence reflect past limnological conditions and have been widely used as climate proxies in high-altitude Himalayan palaeolake sediments [97–101].

The measured environmental magnetic parameters are also sensitive to magnetic grain size variations, and, subsequently, the determination of environmental changes at the site and depositional environments [89–91]. The magnetic grain size and thus domain structure of iron minerals in sediments range between multidomain (MD), stable single domain (SSD or SD), pseudo-SD (PSD), and superparamagnetic (SP) grains. Information about the magnetic grain size in sediments can be used to identify sediment provenance areas [102,103]. We describe here the magnetic mineral data with reference to the pollen zone constituting the sediment profile. This has been carried out to identify the similarities and significance of the magnetic data and the palynological interpretations.

Inferences were further drawn to highlight the changes occurring in the Late Holocene climate at the Zemu glacier, North Sikkim, and their regional and global teleconnections to other existing proxy-based qualitative and quantitative records.

2. Materials and Methods

Study Sites, Environmental Setting and Vegetation

The Sikkim Himalayas are occupied by glacierized basins, mostly in the western and northern regions of the state. Most of these glaciers drain their water into the Tista River and are commonly termed Tista Basin glaciers. The four main glacier basins are the East Rathong basin, Talung basin, Changme Khangpu basin, and Zemu basin, covering about 7172.21 km^2. Among these, the Zemu Basin occupies an area of 2391.60 km^2, covered by 250 glaciers. This basin contributes to two major tributaries, the Zema Chhu ('Chhu': river) and Hema Chhu [104]. The Zemu Chhu is the main feeder of the river Tista. The present study site is situated in the Zemu glacier basin, North Sikkim (Figure 1), which is part of the eastern Himalaya region. The Zemu glacier lies on the eastern face of Kanchendzonga peak and is the largest (41.2 km^2) and longest (28 km) glacier in the Sikkim Himalaya region [105]. The Zemu glacier originates from the eastern flank of the Kanchendzonga ridge. The glacier flows in an easterly direction, draining towards the northern slopes of Simvo and Sinialchu. The glacier has many trenches on its northern and southern sides between the lateral moraine ridges and the rock wall [106]. These trenches have arisen due to the lateral shrinkage of the glacier [106,107]. The Zemu glacier region is situated towards the north of the Main Central Thrust (MCT) and is composed of Kanchenjunga Augen-Gneiss. The porphyritic augen-gneisses with streaks of biotite are recorded towards the north of Lachen [108]. Bands of calc-gneisses stratified along with the augen-gneiss exist near the Zemu-Lachen confluence. In the northern region of Sikkim, there are many granitic masses and aplitic veins found from Chungthang in the Tista valley to Jakthang in the Zemu valley. There are also granite and pegmatite veins ranging from 1 cm to 1 km in thickness between Chungthang and Lachen [104].

Sikkim is influenced by monsoon winds originating from the Bay of Bengal. The Bay of Bengal lies towards the south of the Sikkim Himalaya and brings more rainfall to the region from May to October. The high elevations are also under the influence of the Tibetan Plateau, which plays an important role in generating the Asian monsoon and influences the atmospheric circulation due to the freezing and thawing of the plateau [109,110]. The topographical variations along the Teesta valley give rise to a mostly humid climate within the mountainous walls of the region [111]. Apart from two meteorological stations, Gangtok and Tadong, where fully-fledged meteorological observatories have been functioning since 1957 and 1978, respectively, other stations are mainly rain gauge stations, and records are available from approximately 4 to 25 years ago [111] (Figure 2). The majority of the state receives heavy rainfall throughout the year, while the months of October–March remain comparatively drier. The mean annual rainfall is minimum (82 mm) at Thangu, North Sikkim, and maximum (3494 mm) at Gangtok. Places with an altitude of 6065 m and above are snowbound, and places as low as 3002 m come within the snowline in the winter. The temperature in the lower altitudes fluctuates between 4 °C and 35 °C, and the temperature of places with moderate altitudes (around 1829 m), such as Gangtok, varies between 1 °C and 25 °C. In high-altitude areas (above 3993 m), the temperature never rises above 15 °C and slides down to freezing point in winter [104].

The vegetation of Sikkim has three discrete botanical zones: tropical, temperate and alpine, distributed according to the elevation and characteristics of the vegetation [112]. The vegetation of the state is classified as low, middle, and upper hill forests, followed by rhododendron-conifer zones and Alpine scrubs and grassland [112]. The present study area falls under *Rhododendron*-conifer (cold temperate or sub-alpine zone, 2700–3600 m) and alpine scrub and grasslands (3600–4300 m and above). The dominant tree taxa along the sampling sites are mostly conifers: *Abies densa*, *Juniperus recurva*, *Larix griffithiana*, *J. squamata*, *Picea spinulosa*, and *Tsuga dumosa*, and broad–leaved taxa: *Betula utilis* and *Rhododendron* spp. At the termination of the tree line above 3600 m, *J. pseudosabina* and *J. recurva* grow as scrubs on hill slopes. The stunted height of *Rhododendron* spp was observed growing on exposed rock crevices at altitudes of 3600 m or above. *Ephedra gerardiana* were found growing only on the hilltops around Thangu. A few species belonging to genera

such as *Ranunculus*, *Anemone*, *Delphinium*, *Rhus*, *Potentilla*, *Primula*, *Fragaria*, *Cassiope* and *Allium* were seen on the gentle slopes of open meadows. The detailed vegetation of Zemu Valley in Sikkim Himalaya has been thoroughly enumerated by Smith and Cave [113].

The detailed methodology for the present study has been described in the Supplementary Information for surface and sub-surface sediment sampling, pollen analysis [114–116] of modern and fossil pollen, mineral magnetism analysis [89–91], chronology, and age-depth model [117], modern climate [111,118–120], numerical analysis [38,70,72,73,76,77,121–123], and palaeoclimatic reconstruction [124–131]. We further describe the results obtained from these particular analyses of the samples collected from Zemu glacier region and its surroundings.

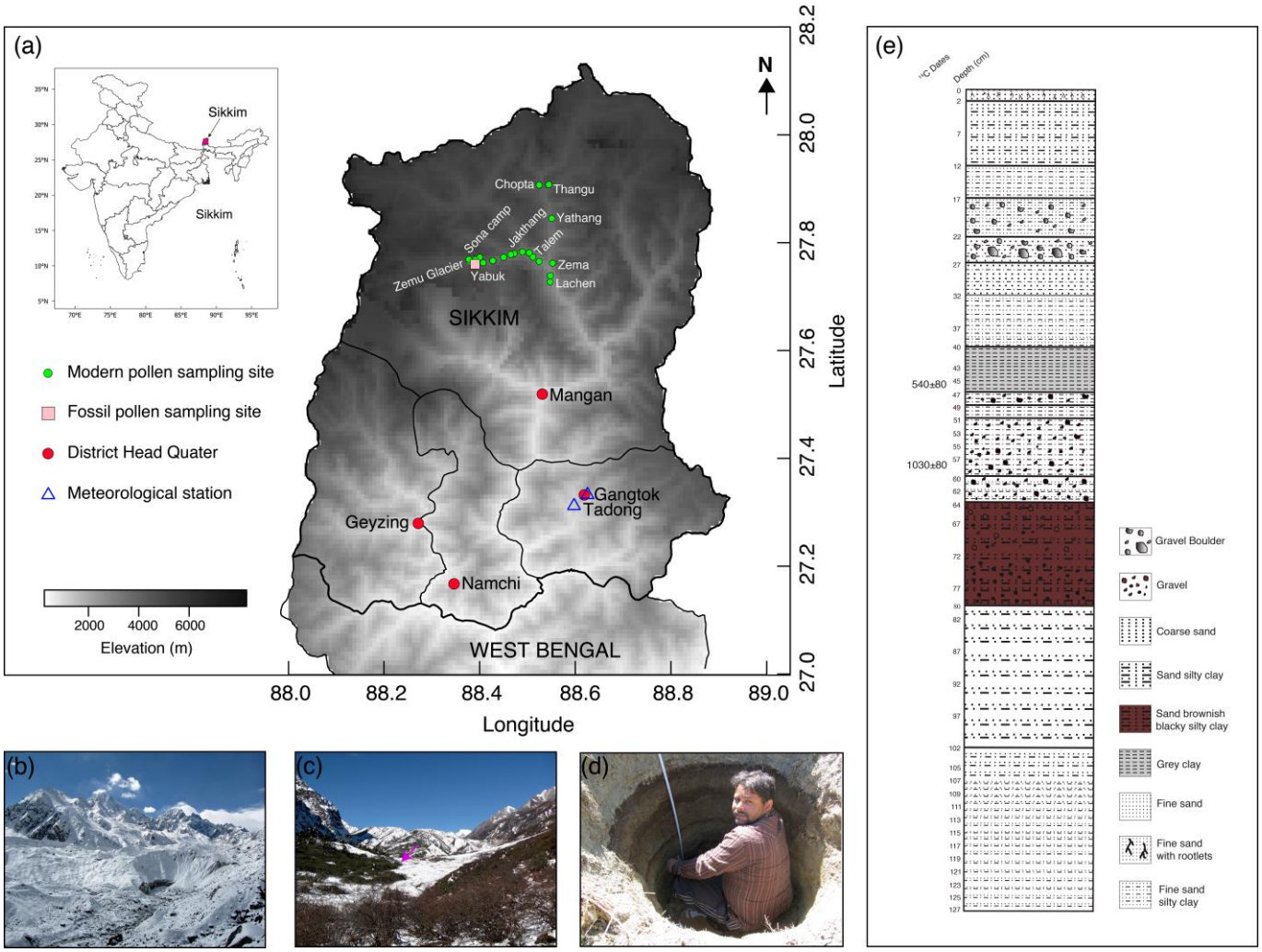

Figure 1. (**a**) Site map showing location of modern pollen sites, fossil pollen site, and meteorological stations are having temperature and precipitation records. (**b**) Snout of Zemu Glacier. (**c**) Broad landscape of the fossil pollen sampling site. (**d**) Sampling trench for sediment collection and (**e**) fossil sampling profile.

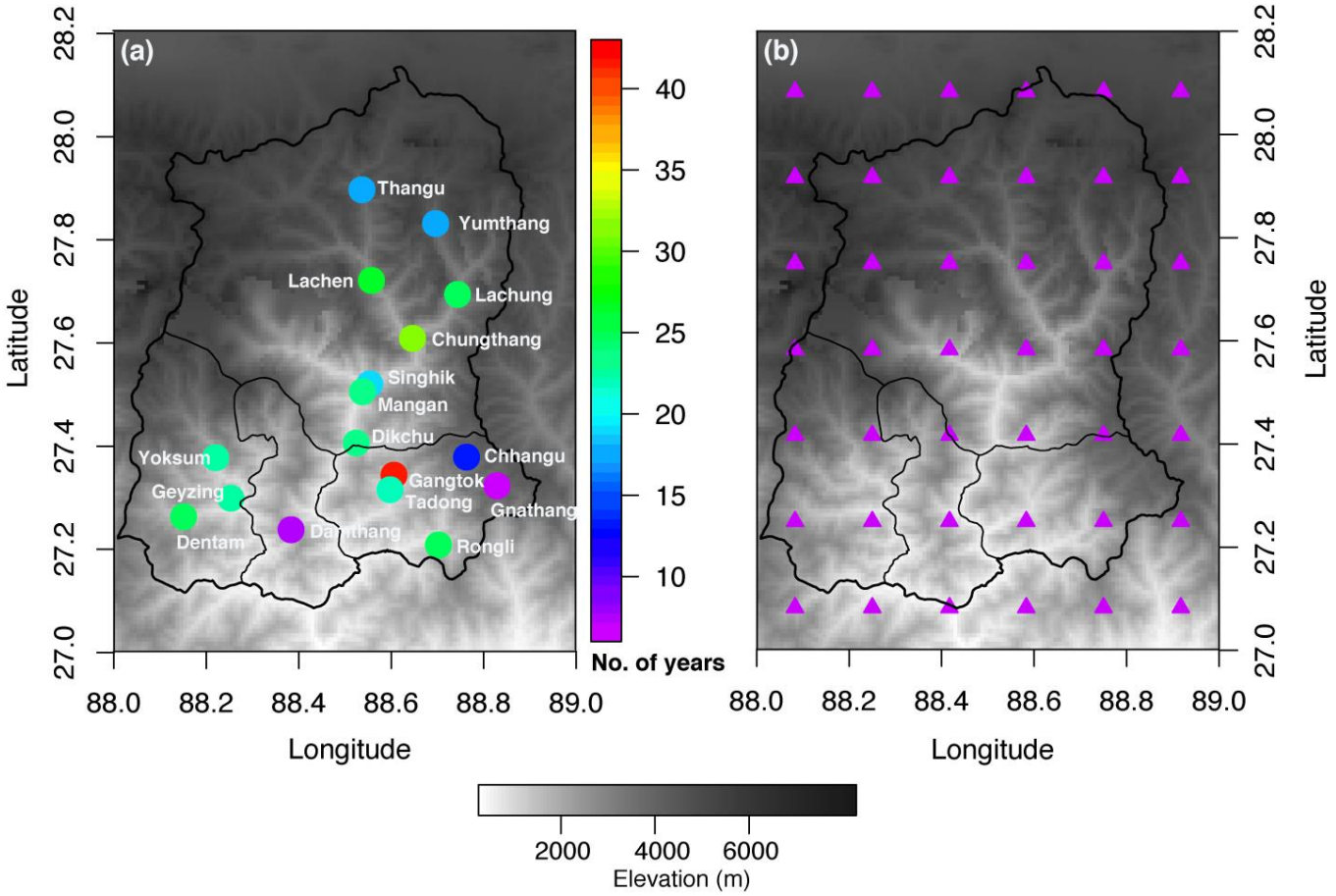

Figure 2. Distribution of (**a**) precipitation meteorological station network with number of years records. (**b**) The CRU 10 min climate grids points used to interpolate the modern climate data of modern surface pollen sites. The map is generated using digital terrain elevation dataset SRTM30 (http://srtm.csi.cgiar.org, accessed on 10 January 2022).

3. Results

3.1. Modern Pollen Sites and Assemblages

The modern pollen sampling sites considered in the present study are well represented in the north-west transect (Lachen to Zemu Glacier) but the densities are relatively low in the northern transect of Lachen towards Thangu (Figure 1). These sites cover vegetation zones ranging from sub-tropical to temperate to alpine, with both coniferous and broad-leaved elements. The climatic variation of these sites ranges with gradients in MAT (1.4–10.6 °C), MTCO (−7.4–2.6 °C), MTWA (9–16 °C), MAP (61–145.5 mm), and elevation (2600–4311 m) based on gridded climate data sets (Figure 3). The details of the gridded climate data have been described in Supplementary Information.

3.2. Ordination

The unconstrained ordination using PCA showed that the first two axes capture 49.1% (axis 1, 31.1%; axis 2, 18.0%) of the total variance. This suggests that only a few variables dominate the data structure, but they are considered high in such high-elevation and climatically contrasting regions. The constrained ordination using RDA with pollen and climate data (MAP and MTWA) showed the eigen values of the first and second axes are 0.1444 and 0.0421, explaining 77.43% of the total variance in the pollen assemblage data (Figures 4 and 5). The RDA was also carried out with MAP and MTWA separately. The first RDA axis captures 12.23% variance in the pollen datasets and shows significant correlation with MAP ($r = 0.696$, $p < 0.02$), while with MTWA, the first axis captures 9.93%

variance with significant correlation (r = 0.667, $p < 0.046$). The RDA with MAP and MTWA variables shows a similar pattern to the PCA, suggesting that both the variables have a strong influence on the underlying structure of the modern pollen data.

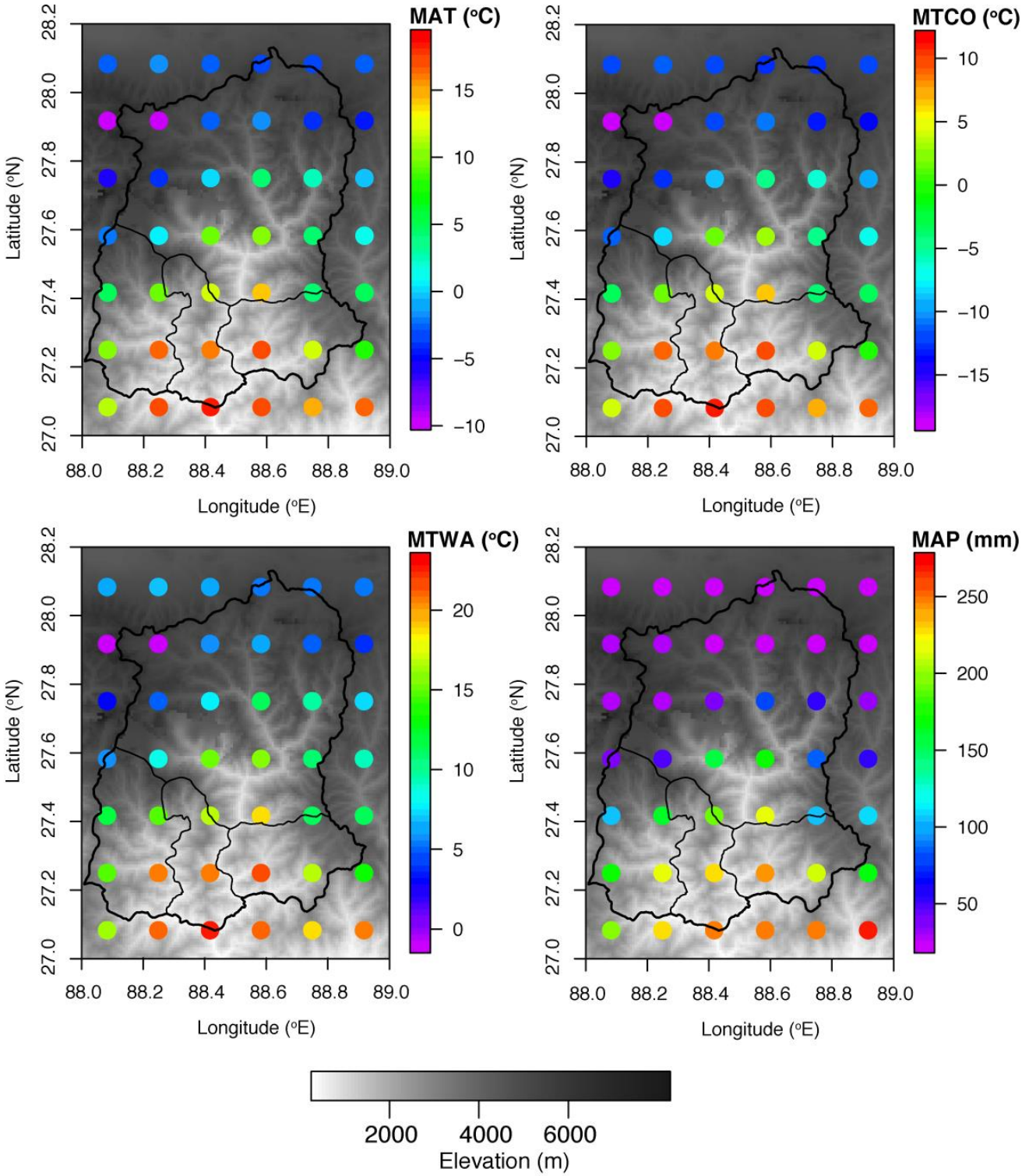

Figure 3. Range of climatic variation of CRU 10 min climate gridded data (MAT, MTCO, MTWA and MAP) in Sikkim and its vicinity along with elevation gradient. The map is generated using digital terrain elevation dataset SRTM30 (http://srtm.csi.cgiar.org, accessed on 10 January 2022).

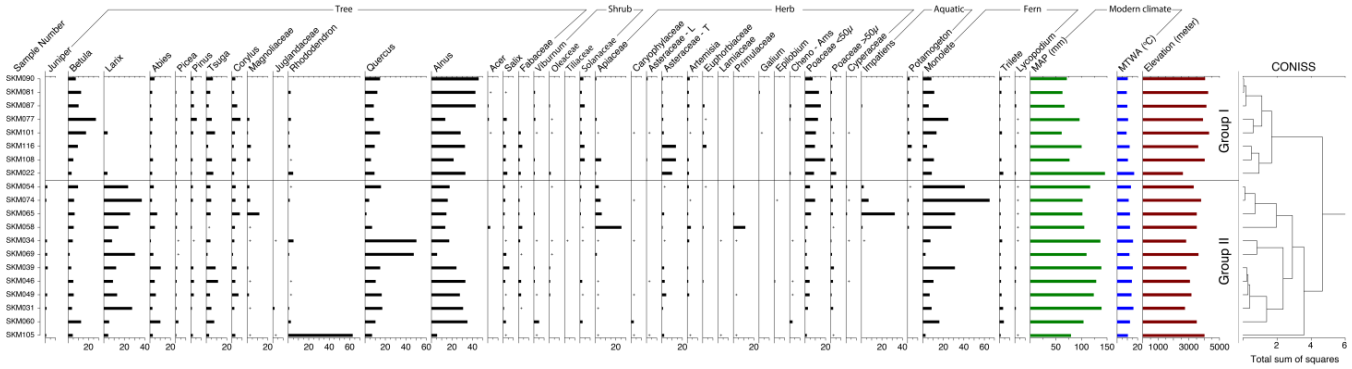

Figure 4. Pollen spectra showing modern pollen distribution from North Sikkim, eastern Himalaya along elevation and estimated MAP, MTWA for modern pollen sampling sites.

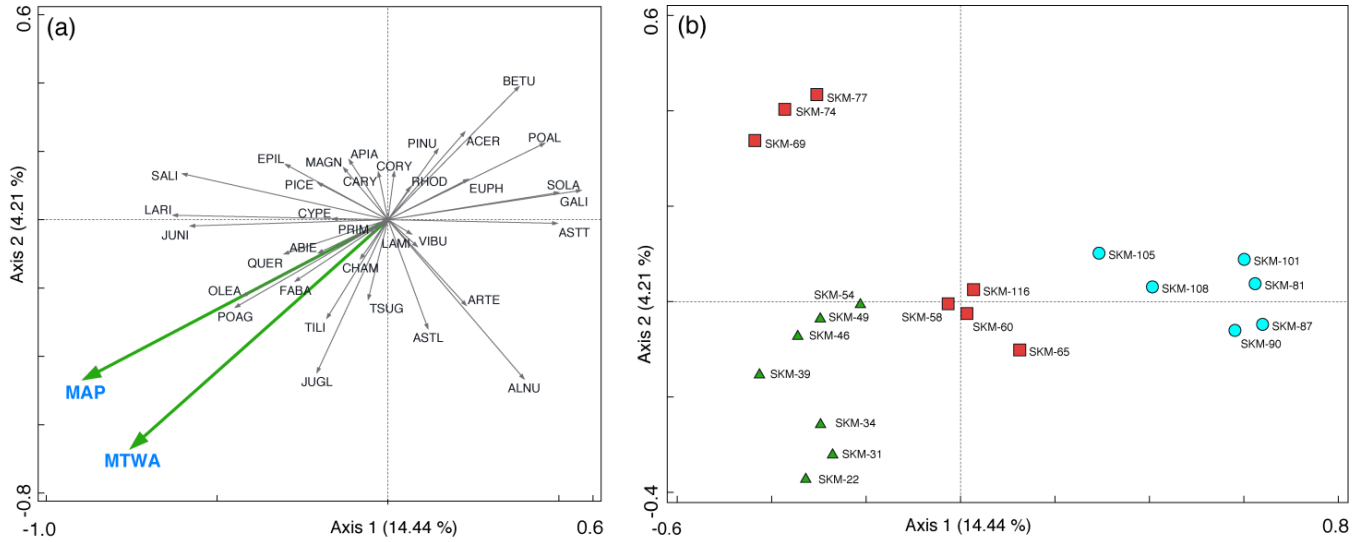

Figure 5. (**a**) Ordination (Redundancy Analysis, RDA) diagram of climates and modern pollen spectra. (**b**) Distribution of modern pollen sampling sites showed by RDA.

In RDA, some pollen taxa are grouped together and some are separated (Figure 5). The RDA axis 1 segregated coniferous taxa (Juniper, *Larix*, *Abies*, *Picea* and *Tsuga*) and broadleaved taxa (Juglandaceae, *Quercus*, *Salix*, Fabaceae and Oleaceae) on the left side. The coniferous taxa (*Pinus*) and broadleaved taxa (*Betula*, *Alnus*, *Acer*, *Corylus*, *Rhododendron* and Magnoliaceae) were separated on the right side of axis 1. It was shown that apart from *Pinus*, all other conifer taxa were grouped together by axis 1. The RDA axis 1 also differentiated in the pollen assemblage of wild grass (Poaceae < 50 µ) and cultivated grass (Poaceae > 50 µ) on two sides of the axis. Most of the shrub and herb elements were concentrated in the center of the ordination and did not show clear segregations.

The modern pollen sites were separated in RDA according to climatic influence (Figure 5). The first RDA axis segregates sites with MAP (60.9–79.0 mm) and MTWA (9.0–10.3 °C) from sites with MAP (116.5–145.5 mm) and MTWA (13.2–16.4 °C). The sites separated by RDA axis 1 are comparable with the altitudinal gradient. The sites (SKM081, SKM087, SKM090, SKM101, SKM105 and SKM0108) segregated on the right side of axis 1 (Figure 5) have low MAP and MTWA, are from a higher elevation (4016–4311 m), and are mostly closer to the Zemu glacier and within its vicinity, which is in an alpine climate. The sites (SKM022, SKM031, SKM034, SKM039, SKM046, SKM049 and SKM054) with high MAP and MTWA segregated on the left side of axis 1 (Figure 5) are mostly from a lower elevation (2600–3303 m) and are influenced by a cool, temperate climate. The sites (SKM058, SKM060, SKM065 and SKM116), which are laid in intermediate and close to

the center of both axes, and sites (SKM069, SKM074, SKM077), isolated on the left side of axis 1, are mostly influenced by both the higher and lower elevation climatic conditions of the region, with moderate MAP (95.9–109.7 mm) and MTWA (10.5–12.5 °C). The altitudinal gradient of these sites ranges from 3501 to 3915 m, with a sub-alpine climate, and seems segregated under the influence of RDA axis 2 (Figure 5). Similar segregation was observed when the modern pollen data were grouped in zonation (Figure 4) using unconstrained chord-distance clustering (CONISS) on a square-root-transformed modern pollen percentage assemblage.

3.3. Chronology and Palaeo–Vegetation History

Based on the derived chronology using linear regression, the Yabuk sediment profile covers the last 2992 cal years BP (1042 BC), confirming that these sediments belong to the Late Holocene. So, the present fossil records represent the vegetation and climate records since the Late Holocene. The chronology detail of the fossil sediment profile is provided in Table 1. The rate of sedimentation calculated was mostly similar from top to bottom in depth, and its average rate was 0.08 cm/year.

Table 1. Radiocarbon ages and calibration.

	YABUK 12	YABUK 18
Depth (cm)	46	58.5
14C Radiocarbon age	540 ± 80	1030 ± 80
Calibrated age (cal yrs BP)	566	945
Calendar age (BC/AD)	1384	1005

Based on the CONISS of the percentage of pollen data, three zones, YAB–I, YAB–II and YAB–III, were established to represent the major phase of vegetation change. Two zones, YAB–II and YAB–III, are further divided into two sub-zones to represent the minor vegetation changes within the broad phase (Figure 6). The vegetation changes in each zone are described in Supplementary Information.

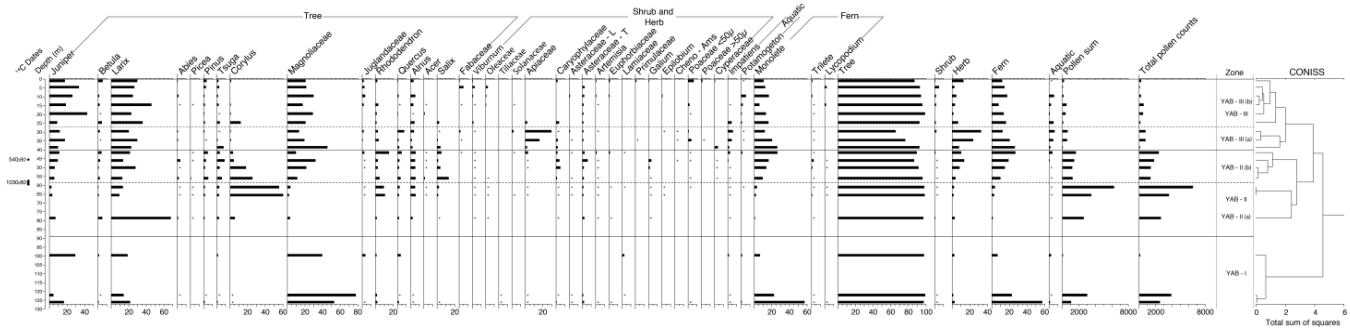

Figure 6. Pollen diagram of sediment profile from Yabuk, North Sikkim, eastern Himalaya along with zone prepared using CONISS.

3.4. Pollen–Climate Calibration and Transfer Function

The RDA shows that there is a statistically significant relationship between modern pollen assemblages and the climatic variables MAP and MTWA (Figure 5). A transfer function was developed for MAP and MTWA as these were the significant climatic variables entered in the ordination analysis, RDA. Prior to final model development, we found four samples (SKM022, SKM069, SKM074 and SKM101) producing extreme values in the analyses. These sites were removed from the training set prior to performing PLS regression and calibration. The improved pollen-climate PLS transfer function was finally developed based on the screened dataset (Table 2). The performance of transfer function models for MAP and MTWA assessed with components retained in the PLS regression approach

and assessed by leave-one-out cross-validation showed the sixth component for MAP and the fifth component for MTWA to be the best performing models (Table 2, Figure 7). The sixth component of MAP showed the lowest value (17 mm) of RMSEP and the highest value (0.585) of r^2 between observed and predicted MAP (Table 2). A strong relationship ($r^2 = 0.993$, $p < 0.01$) was observed between observed MAP and the values predicted for the study sites based on observed MAP (Figure 7). In the case of MTWA, the fifth component showed the lowest value (1.1537 °C) of RMSEP and the highest value (0.696) of r^2 between observed and predicted MTWA (Table 2). A strong relationship ($r^2 = 0.982$, $p < 0.01$) was observed between the observed MTWA and the values predicted for the study sites based on the observed MTWA (Figure 7). A comparison of observed MAP and MTWA and residuals (predicted minus those observed for MAP and MTWA) showed that the calibration model predicts values relatively well within the range of observed MAP and MTWA (Figure 7).

Table 2. Model performance statistics as assessed by leave-one-out cross-validation for the using first x (x = 1–6) components of the partial least square regression (PLS). Component marked with * are used for further analysis and for climate (MAP and MTWA) reconstruction.

	Apparent		Cross-Validated (Leave-One-Out)	
PLS Component	**RMSE**	**Correlation (r^2)**	**RMSEP**	**Correlation (r^2)**
MAP				
Component 1 a	19.017	0.479	23.593	0.235
Component 2 a	14.034	0.717	25.818	0.207
Component 3 a	11.679	0.804	27.380	0.213
Component 4 a	9.412	0.873	33.026	0.129
Component 5 a	7.650	0.916	36.318	0.116
Component 6 a	6.674	0.936	38.949	0.105
Component 1 b	13.061	0.734	18.501	0.473
Component 2 b	8.783	0.880	18.918	0.480
Component 3 b	5.574	0.952	18.699	0.505
Component 4 b	4.062	0.974	18.688	0.514
Component 5 b	3.558	0.980	17.103	0.580
Component 6 b *	2.193	0.993	17.076	0.585
MTWA				
Component 1 a	1.651	0.439	2.103	0.158
Component 2 a	1.198	0.705	2.180	0.176
Component 3 a	0.991	0.798	2.230	0.214
Component 4 a	0.794	0.870	2.641	0.133
Component 5 a	0.642	0.915	2.918	0.121
Component 6 a	0.562	0.935	3.084	0.109
Component 1 b	0.942	0.792	1.381	0.555
Component 2 b	0.604	0.915	1.309	0.609
Component 3 b	0.423	0.958	1.217	0.658
Component 4 b	0.332	0.974	1.215	0.663
Component 5 b *	0.279	0.982	1.154	0.696
Component 6 b	0.174	0.993	1.245	0.657

a Original dataset, n = 20. b Screened datasets, n = 16.

3.5. Late Holocene Quantitative Palaeoclimate Reconstructions

The successful validation of the transfer function models based on standard statistical criteria [38] shows prospects for the quantitative reconstruction of both precipitation (MAP) and temperature (MTWA) variables in the present study. This has led to the reconstruction of MAP and MTWA over 2992 cal years BP (1042 BC) for the Zemu glacier region of Yabuk, North Sikkim, eastern Himalaya (Figure 8). The application of the PLS MAP model using the sixth component to the Yabuk fossil pollen records yielded precipitation values between 98.9 and 144.9 mm. Similarly, for the PLS MTWA model using the fifth component, temperature values between 12.2 and 15.9 °C were yielded. The reconstructions showed

variability during several periods as dry and wet episodes in MAP and cool and warm episodes in MTWA (Figure 8).

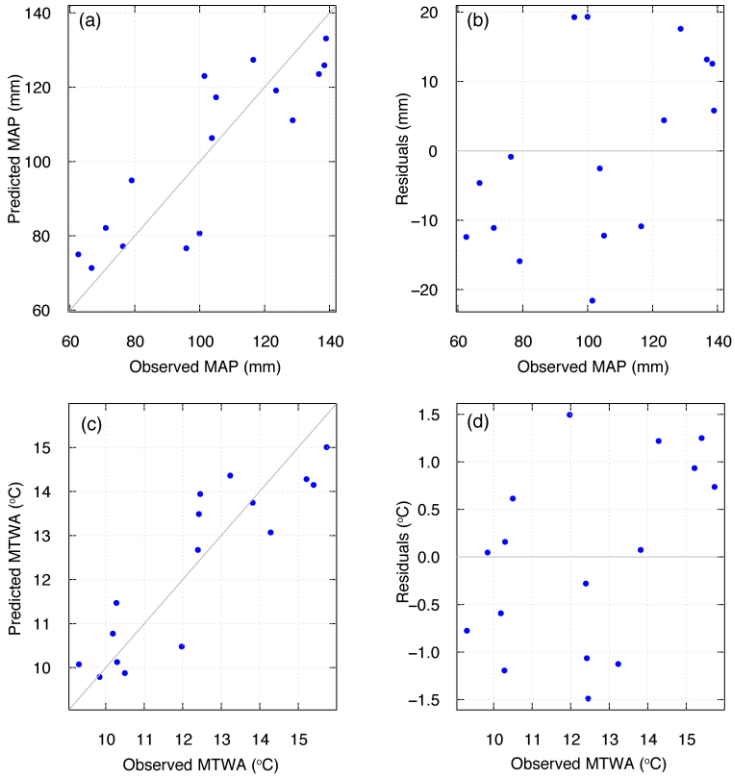

Figure 7. (**a**,**b**) Observed, predicted and residual plot of MAP. (**c**,**d**) Observed, predicted and residual plot of MTWA.

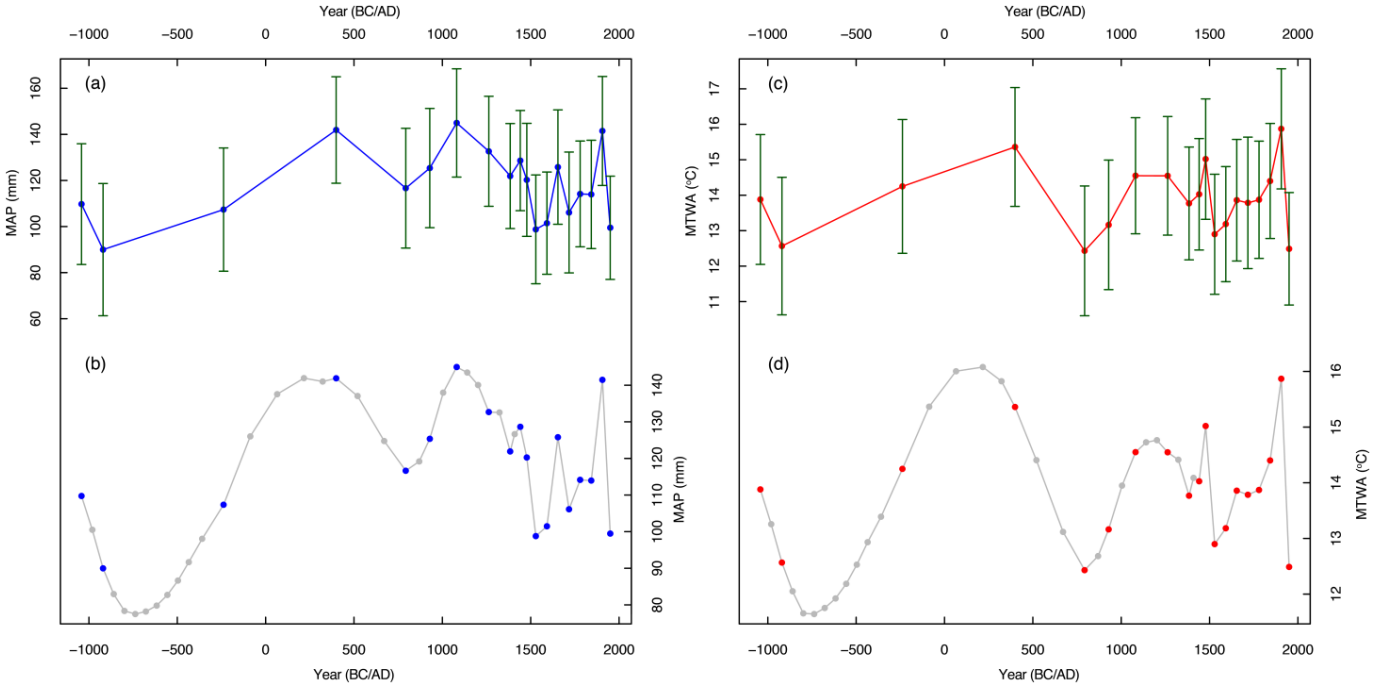

Figure 8. Reconstructed climates (**a**,**b**) MAP and (**c**,**d**) MTWA since 2992 cal years BP (1042 BC). The grey dots in both the figure are interpolated values where the palynomorphs are not recovered.

The reconstructed MAP showed variability during several periods as higher (wet) and lower (dry) episodes (Figure 8). The beginning of the reconstructed MAP, i.e., during 2992–2188 cal years BP (BC 1042–238), shows a lowering of precipitation, with the lowest (90 mm) in 2870 cal years BP (BC 920). The precipitation was higher in 1551 cal years BP and suddenly decreased until 1157 cal years BP (AD 793). Then, high precipitation was observed from 1021 to 742 cal years BP (AD 929–1478), with a maximum peak in 869 cal years BP (AD 1081). The precipitation was lower during 421–107 cal years BP (AD 1529–1843), ranging between 98.8 and 113.9 mm. However, in 296 cal years BP (AD 1654), the precipitation showed a higher value of 125.8 mm. During the recent phase of the reconstructed MAP, it showed an increasing trend in precipitation.

The reconstructed MTWA (Figure 8) shows variability during several periods, such as rising (warm) and lowering (cold) episodes in temperature (Figure 8). The beginning of the reconstructed MTWA, i.e., during 2870–2992 cal years BP (BC 1042–920), shows a lowering of temperature (13.9–12.6 °C). The temperature rises from 1551 to 2188 cal years BP (BC 238 to AD 399), with (14.2–15.4 °C) and then lowered (12.4–13.2 °C) during 1157–1021 cal years BP (AD 793–929). The temperature started rising in 869 cal years BP and reached its maximum in 472 cal years BP (AD 1478) at 15 °C. After this continued warming period, a gradual cooling phase was observed. The temperature slowly lowered in 421–170 cal years BP (AD 1529–1780) to (12.9–13.9 °C). The reconstructed MTWA around 107 cal years BP (AD 1843) shows the advent of warming after the preceding cold episodes.

3.6. Magnetic Parameters, Fossil Pollen and Quantitative Palaeoclimate

The reconstructed quantitative precipitation and temperature records were compared with the pollen zones developed in the fossil data and supplemented with magnetic parameters, which are described in detail in Supplementary Information (Figure 9).

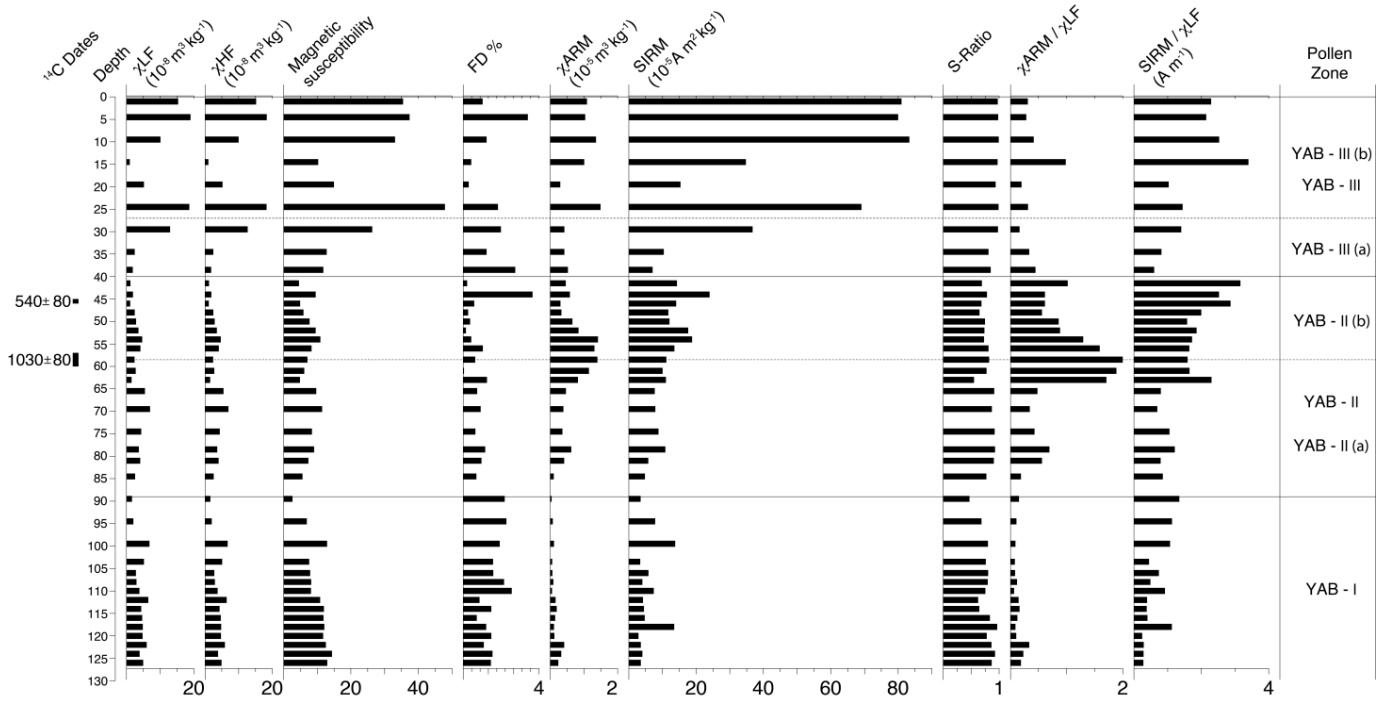

Figure 9. Environmental mineral magnetism records along with pollen based quantitative climate (MAP and MTWA) reconstructions. The zonation represented on the right side of the figure is based on pollen zone given in Figure 6.

4. Discussion

4.1. Modern Pollen Distribution

The samples collected for modern pollen analysis have a distinct pattern of dominance of species that is also segregated also in terms of the variation in the altitude of sampling. The instances of grouping and/or clustering in both CONISS and ordination statistics following the same trends are evident. The first group (Group I) of samples or clusters included higher altitude samples (SKM90, SKM81, SKM87, SKM77, SKM101, SKM116, SKM108), occupying an altitudinal range of (3608–4300 m) and samples (SKM22) of lower altitude (2600 m). These samples showed a high dominance of alpine taxa. However, taxa such as *Tsuga*, *Quercus* pollen, and a few instances of *Larix* pollen were also present, probably arriving from adjoining regions.

In the second group (Group II), the samples (SKM54, SKM74, SKM65, SKM58, SKM34, SKM69, SKM39, SKM46, SKM49, SKM31, and SKM60) collected at various sites in the valley had an altitude range of 2800–3700 m. These sets of samples recorded the dominance of subalpine tree taxa, a few shrubs and herbs, and larger grass pollen and aquatic taxa. This variation in taxa can again be attributed to the lower temperatures at this altitude and increased soil moisture due to snow melt and a higher amount of precipitation. This sampling area is exposed to variable climatic conditions, allowing mixed species to appear in the sediments. However, a slight shift towards higher altitude taxa cannot be overruled. There is one sample (SKM 105), which was collected from the distant region of Chopta Valley, that has similar taxa but high levels of *Rhododendron* in the sample, consequently forming a separate node in the second group or cluster of samples. However, the ordination statistics and RDA imply considerations for species grouping, including climatic parameters. Hence, it is imperative that all the data and sample groups are separated not only based on the species and climate variables (MAP and MTWA), but also according to the altitude of sampling. To further strengthen the results of RDA, the CONISS results are also comparable, giving a definitive pattern to the species distribution in the region.

4.2. Pollen–Climate Relationships

The relationship between pollen assemblages and the environmental variables established using the ordination method showed the significant influence of MAP and MTWA on vegetation. The climatic variable MAP with axis 1 showed a high correlation compared to MTWA, which is slightly less correlated with axis 1, but both are statistically significant ($p < 0.05$). This suggests that the control of precipitation over the distribution of surface pollen could be the primary environmental driver controlling vegetation and species variations. It has been observed that sites with arid or semiarid climatic conditions, with vegetation cover and composition, are mostly controlled by moisture availability [62]. The analysis of the satellite-based normalized difference vegetation index (NDVI) compared with rainfall data from states in India showed a strong relationship between them. The study showed that NDVI is affected positively by the amount and intensity of rainfall [88]. This relationship is stronger during the monsoon season, the period that contributes the maximum percentage of water availability in annual rainfall. The NDVI precipitation result also supports the fact that precipitation has a stronger effect on vegetation distribution in the present high-elevation study area of the eastern Himalayas. In North Sikkim, precipitation in the form of rain or snow occurs throughout the year. Thus, in the present study region, precipitation has a strong influence throughout the year, which supports the present findings that highlight the significant influence of precipitation on the regional vegetation. However, in Sikkim, the rainfall/precipitation decrease sharply at higher elevations (>2000 m) in all seasons except during winter [111]. Hence, the availability of soil moisture for most taxa is high at all times, either due to rainfall or snow. However, due to the variation in altitude, the precipitation and temperature distribution at all sampling sites vary within a wide range. In the glacier region (>4000 m), the temperature decreases with snow cover, and precipitation also loses its intensity. In the cool, temperate region (2600–3300 m), both precipitation and temperature are usually at their peak during the

south-west monsoon months (June to September). The rise in temperature could lead to high evapotranspiration and become the limiting factor for vegetation. The significant relationship observed with temperature could be possible, because the growth of the plants varies greatly along both latitudinal and altitudinal gradients. In the present study, the influence of both temperature and precipitation might be due to the fact that both temperature and precipitation vary greatly with altitudinal gradients. Due to this altitudinal-climatic distribution, both temperature and precipitation become the important limiting factors for the growth of plants in this region. The altitudinal influence on climate cannot be ruled out in mountainous and high-altitude regions. As the elevation increases, the temperature decreases in most of the mountainous region [4,132,133], in addition to precipitation, as also observed in the present study sites (Table S1) and reported for the entire region of Sikkim by [111]. Similar inferences on pollen–temperature–precipitation have been observed from adjoining regions such as the Tibetan Plateau, China, and Mongolia [57,59,62,134–137] on modern pollen-climate calibration, along with the statistical parameters observed in the transfer function model. The influence of precipitation as a primary environmental factor can also be explained by the fact that modern pollen sites are located in high-elevation areas with arid or semiarid climatic conditions, where vegetation cover and composition are mostly controlled by moisture availability.

4.3. Environmental Geomagnetism and Climate Reconstruction

The reconstruction of mean annual precipitation (MAP) has been based on magnetic minerals within a soil in various studies using different quantitative techniques [96,138–142]. Magnetic minerals such as magnetite/maghemite, hematite, and goethite abundances in soils have been identified to have a quantitative relationship with precipitation [96,142,143]. Magnetic palaeo-precipitation proxies have been studied widely in the Quaternary to recent Loess–paleosol systems in China [138,144], New Zealand [145], Alaska [146], North America [147–149], and Russia [150,151]. These records exhibit that the relationship between magnetic minerals and MAP differs spatio-temporally [96]. The Loess–Paleosol sequences of China have shown that variation and aeolian dust fluxes are influenced by regional monsoonal climate patterns and increases in pedogenic processes due to high precipitation and temperature [96,138,152–154]. Thus, the strong relationship between iron oxide mineralogy in soil sequences and climatic variations has been well established globally [96]. However, the magnetic palaeo-precipitation proxies used to estimate MAP have been said to have certain uncertainties [96,155,156].

In this study, we do not attempt a direct palaeo-precipitation reconstruction using mineral magnetic data. We have attempted to make a comparison of the reconstructed MAP using palynological data with magnetic mineral variations. Mineral magnetism data are an additional tool to identify the variations in the palaeoclimate of the Zemu glacier. Similar variations comparable to the reconstructed climate (MAP, MTWA) at Zemu glacier were found. There were many controlling factors, such as soil moisture, glacial melt, detrital deposition, podogenic processes, and regional sediment influx at the Zemu glacier. All these factors, along with the climatic parameters, control the magnetic mineral variations in the sediment. Here, the fossil pollen data also correspond to vegetation changes along with climatic variations at the Zemu glacier. The fossil pollen data in zone YAB–I is less, but an increase in the ferromagnetic mineral content is concurrent with the high MAP and MTWA and high pollen counts. In the other two zones, the vegetation gives a pattern similar to the changes in MAP and MTWA, along with the mineral magnetic. The glacier also demonstrated changes regarding the type of sediment influx at the sampling site during high precipitation periods in zones YAB–II and YAB–III, which are composed of coarse gravel with sand and silty clays. Such changes are visible in the lithology profile of the samples collected near the Zemu glacier. It is evident that material coming down from the snout of the glacier and the surrounding topography influenced the magnetic mineralogy. The vegetation, climate, and sediment flux in the valley during the Late Holocene are clearly linked together in our record. Both palynological and environmental geomagnetic data

provide strong evidence of the influence of MAP and MTWA as climatic factors working in the Zemu glacier valley.

The environmental magnetism parameters are significantly low in terms of their numerical values throughout the sediment profile. They successfully capture the signals and oscillations in the environment and climate at the Zemu glacier. These parameters were analyzed for all the samples, which included samples not analyzed for palynomorphs due to the high sand content. Though we managed to obtain the entire profile data, it is possible that including all the sample data reduced the possibility of easily identifying the magnetic behavior of the minerals in the profile. However, it was important that we supported our climatic interpretation and reconstruction based on other supportive evidence.

4.4. Evaluation of Climate Reconstructions

The climate of the Late Holocene, especially the last 1000–1500 years, sets the background for 20th-century climate warming. The climate records during this period are required to perceive the natural variability in the climate system. The proxy-based long climate records emphasize the interest in quantitative climate data beyond the range of instrumental records. Long-term climate reconstructions derived from various well-dated proxy data indicate that the past millennium is the best documented interval with both historical and climate data [157]. The present pollen-based quantitative climate (MAP and MTWA) reconstructions successfully captured well-known global climate events of the recent millennium. These climatic signals helped us assess the background for recent century-long climate warming in the largest glaciated region of the eastern Himalayas.

In the present reconstructed MTWA, the high temperature covering the time span of 929–472 cal years BP (AD 1021–1478) is comparable with the MWP. After attaining a gradual rise in temperature during 509–472 cal years BP (AD 1441–1478), the significant lowering of temperature until 421 cal years BP (AD 1529) could be related to the cooling period near the beginning of the LIA. This cooling period observed in the present MTWA reconstruction is comparable with a widely known event, the Spörer Minimum, observed during AD 1460–1550 [158]. Jiang and Xu [158] clearly demonstrate that if the Spörer Minimum extended from AD 1460 to 1550, it could be a specious result; if its extent was AD 1400–1510, it could be determined as an actual feature of solar variability during that time. The slight decrease in temperature after attaining the increasing trends in our MTWA reconstruction during 296–233 cal years BP (AD 1654–1717) is comparable with a cold event widely known as the Maunder Minimum (AD 1645–1715) in the middle of the LIA [159]. The Maunder Minimum refers to a period of low solar activity [160]. The physical link between low sunspot activity and cooling temperatures has not been established, but the coincidence between the Maunder Minimum and the deepest trough of the LIA is suggestive of such a connection [161]. The present reconstructed MTWA has not captured this event significantly compared to the Spörer Minimum. Thus, the overall lowering of temperature covering a time span of 421–170 cal years BP (AD 1529–1780) suggests that the LIA event was present around the Zemu Glacier Valley. The LIA episodes observed in the reconstructed MTWA showed a sudden decrease in temperature in the early part of the initiation of the cold period, and gradually the temperature increased, with a slight decrease during the middle of the LIA. The reconstructed temperature around 107 cal years BP (AD 1843) shows the arrival of warming after the cold episodes of LIA in the Zemu glacier valley and is similar to the Current Warming Period (CWP).

The reconstructions from our records captured comparable well-known climatic events (MWP and LIA), but the timing identified is indeed not the same as that recorded in various studies (described in Sections 4.5 and 4.6). The MWP was a time of warm climate during AD 1100–1300, which peaked in the 11th century and ended abruptly around 1300 AD [8]. Similarly, the LIA event is a known widespread climatic cooling event that lasted approximately from the 14th to the 18th centuries AD [12]. Later, Mann et al. [10] argued that MWP might be related to other climate events around the world and occur from about AD 950 to 1250, and that the cooling event LIA lasted from AD 1400 to 1700.

However, Graham et al. [11] reported the duration of MCA/MWP as ca. 900–1350 AD and the LIA as ca. 1500–1850 AD. The present climate reconstruction shows cool (dry) and warm (wet) variability within the LIA and MWP, respectively. We observed cold (dry) climatic records punctuated within the 'warm (wet)' period of MWP. Similarly, warm (wet) records are observed during the 'cool (dry)' period of LIA. This illustrates the fact that 'Medieval Warm Period' and 'Little Ice Age' are moveable terms depending on region. However, the present finding supports that the worldwide climatic variability of MWP with a warm (wet) climate and LIA with cold (dry) periods also exists in this remote region of the Zemu glacier valley in the eastern Himalayas. Wanner et al. [162], based on a synthesis review of mid-to-late Holocene global climate change, concluded the existence of warm and cold periods, especially hemispheric-scale warming leading to the MWP and subsequent cooling into the LIA. The possible role of this climatic variability could be due to various natural factors. These could be fluctuations in solar activity, large tropical volcanic eruptions, internal variability in oceanic oscillations, including the El Niño Southern Oscillation (ENSO) and the North Atlantic Oscillation (NAO), changes in the thermohaline circulation, and complex feedback mechanisms between the ocean, atmosphere, sea ice, and vegetation [162]. The strong coupling between the biogenic proxies and reconstructed total solar irradiance during the last millennium from the northeastern Arabian Sea also suggested solar control on the intensity of the Indian monsoon and likely the MWP and LIA as well. Moreover, the large eruptions in the tropics and high latitudes were the primary drivers of inter-annual to decadal temperature variability in the Northern Hemisphere during the past 2500 years [163]. Based on the model simulations, Polanski et al. [157] stated that the eastern Himalayas are affected by summer variations in the temperature gradient between the Bay of Bengal and Indian subcontinent and by a zonal band of intensified Indian-East Asian monsoon link north of 25° N.

Apart from these broad global events of MWP and LIA, our climate reconstruction is also comparable with other climatic events that occurred elsewhere in the globe [164] but were not widely explained compared to MWP and LIA. These events were recorded in the reconstruction before the MWP period. The cooling of temperature at the beginning of the reconstructed MTWA (2992–2870 years BP, BC 1042–920) might be linked with the Sub-Atlantic Cold Period (SACP) that occurred during BC 975–250 [164]. The rise in temperature in the present MTWA reconstruction during 2188–1551 cal years BP (BC 238–399) is similar to the Roman Warm Period (RWP) observed during BC 250–AD 450 [164]. Another event known as the Dark Age Cold Period (DACP), which took place during AD 450–950 [164], is also comparable with the cooling events observed in our temperature reconstruction during the later part of 1157–1021 cal years BP (AD 793–929). However, we do not support the claim that these events were strongly captured in our reconstruction due to the fact that the palynological samples are smaller at the beginning of the chronology. However, at the same time, we can argue that the present reconstruction has the ability to capture climatic fluctuations that occurred during the Late Holocene elsewhere. In future studies, the observation can be strengthened with an increase in palynological sample numbers and a higher-resolution chronology. Thus, greater emphasis was given to MWP and LIA events, which were compared with other records in detail.

4.5. Climate Reconstructions Comparison

In the present study, we provide the first quantitative climate (precipitation and temperature) reconstruction of the Zemu glacier valley in the eastern Himalayas using the transfer function model. In order to look at our climate reconstructions of the Zemu glacier from a larger geographical perspective, we compared them with proxies-based climate reconstructions carried out in India and adjoining areas, including south Asian continents and the northern hemisphere. For this comparison, two approaches were considered: (i) qualitative climate inference made from different proxy-based studies and (ii) quantitative climate reconstruction from various proxies available from NOAA data contributors (www.ncdc.noaa.gov, accessed on 10 January 2022) and obtained from

personal contribution on request. For both approaches, comparisons were made for past climatic events and variability recorded during the Late Holocene.

4.5.1. Climate Reconstructions Comparison—Qualitative Approach

The climatic variability during the MWP and LIA time periods recorded in the present pollen-based climate reconstructions is comparable with other pollen and proxy-based studies carried out in different regions of India, the Himalayas, and the adjoining oceanic region. The time span and climatic inference made for the MWP and LIA periods in these studies [16,84,85,87,158,165–204] are presented in Figures 10 and 11, respectively, and are described in the following section. We have given an extensive explanation and comparison of these records in Supplementary Information.

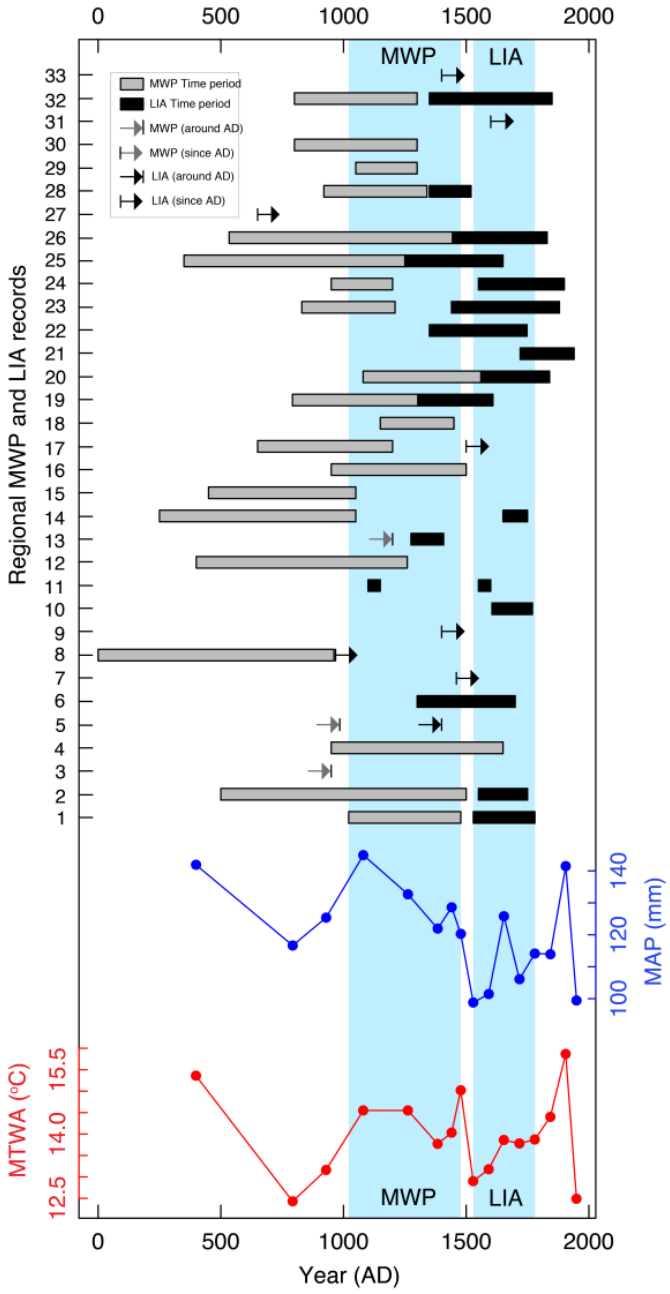

Figure 10. MWP and LIA, time span range (1) Present study (Yabuk, Sikkim, eastern Himalaya), (2) Kupup, Sikkim, eastern Himalaya [85], (3) Khechipiri, Sikkim, eastern Himalaya [84], (4) Jore–Pokhari,

Darjeeling, eastern Himalaya [87], (5) Paradise Lake, Arunachal Pradesh, eastern Himalaya [165], (6) Bhutan, eastern Himalaya [16], (7) Lower Brah Velley, Northeast India [171], (8) West Assam, Northeast India [172], (9) East Nepal [173], (10) Nepal [200], (11) South Central Tibetan Plateau [174], (12) Pinder glacier, Kumaon Himalaya [175], (13) Tipra Bank glacier, Kumaon Himalaya [176], (14) Bhujvas, Gangotri glacier, Garhwal Himalaya [177], (15) Spiti valley, Himachal Pradesh [179], (16) Spiti valley, Himachal Pradesh [183], (17) Parvati valley, Himachal Pradesh [180], (18) Batal, Himachal Pradesh [181], (19) Chandra valley, Himachal Pradesh [182], (20) Badanital Lake, Garhwal Himalaya [184], (21) Uttarkashi, Garhwal Himalaya [185], (22) Chorabari Glacier, Garhwal Himalaya [186], (23) Central Himalaya [187], (24) Sasikul Lake, Pamir [188], (25) Southeast Madhya Pradesh, Central India [191], (26) Southwest Madhya Pradesh, Central India [192], (27) Orissa [193], (28) Central India [194], (29) East Arabian Sea [195], (30) Northwest Arabian Sea [196], (31) Near Oman, Arabian Sea [197], (32) Southeast Arabian Sea [198] and (33) Northeast Arabian Sea [199].

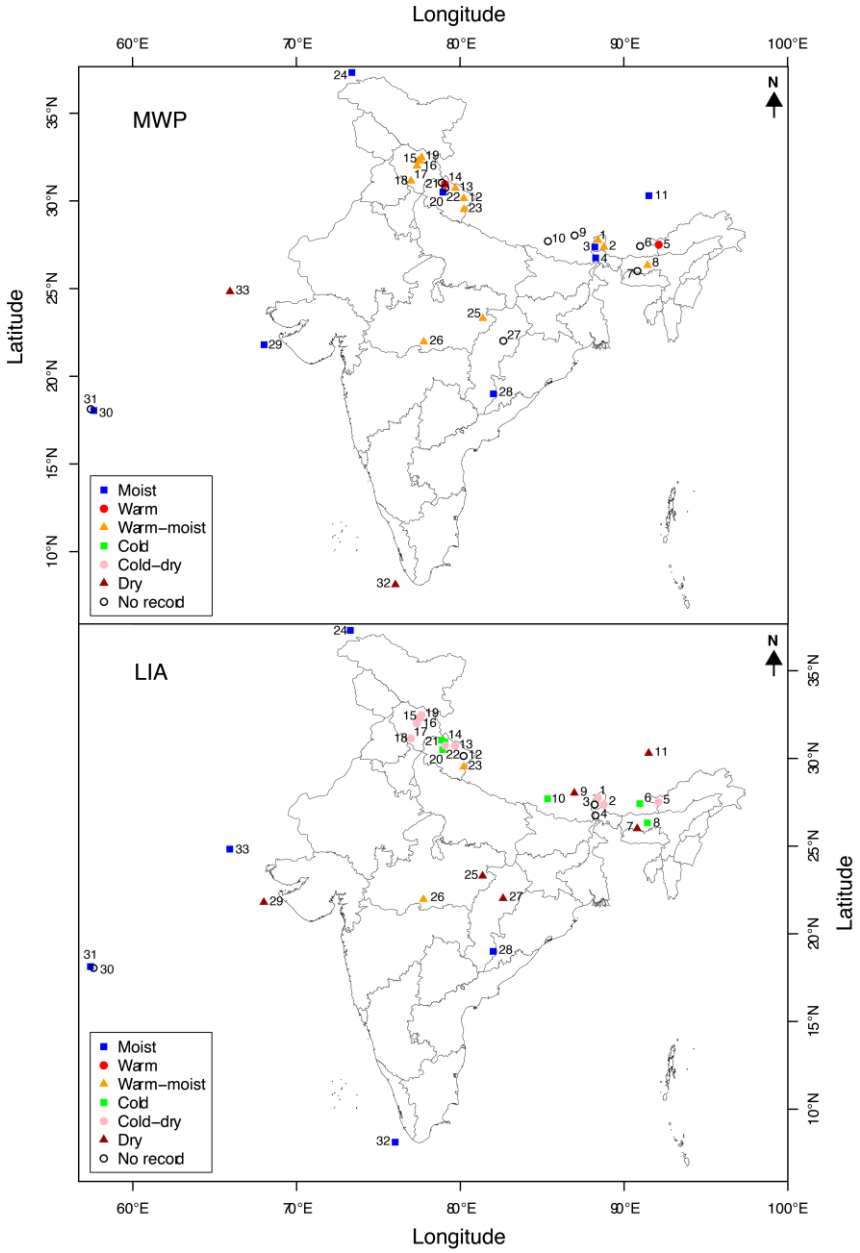

Figure 11. MWP and LIA, climate inference in map with color code (1) Present study (Yabuk, Sikkim, eastern Himalaya), (2) Kupup, Sikkim, eastern Himalaya [85], (3) Khechipiri, Sikkim, eastern Himalaya [84], (4) Jore–Pokhari, Darjeeling, eastern Himalaya [87], (5) Paradise Lake, Arunachal Pradesh,

eastern Himalaya [165], (6) Bhutan, eastern Himalaya [16], (7) Lower Brah Velley, Northeast India [171], (8) West Assam, Northeast India [172], (9) East Nepal [173], (10) Nepal [200], (11) South Central Tibetan Plateau [174], (12) Pinder glacier, Kumaon Himalaya [175], (13) Tipra Bank glacier, Kumaon Himalaya [176], (14) Bhujvas, Gangotri glacier, Garhwal Himalaya [177], (15) Spiti valley, Himachal Pradesh [179], (16) Spiti valley, Himachal Pradesh [183], (17) Parvati valley, Himachal Pradesh [180], (18) Batal, Himachal Pradesh [181], (19) Chandra valley, Himachal Pradesh [182], (20) Badanital Lake, Garhwal Himalaya [184], (21) Uttarkashi, Garhwal Himalaya [185], (22) Chorabari Glacier, Garhwal Himalaya [186], (23) Central Himalaya [187], (24) Sasikul Lake, Pamir [188] [188], (25) Southeast Madhya Pradesh, Central India [191], (26) Southwest Madhya Pradesh, Central India [192], (27) Orissa [193], (28) Central India [194], (29) East Arabian Sea [195], (30) Northwest Arabian Sea [196], (31) Near Oman, Arabian Sea [197], (32) Southeast Arabian Sea [198] and (33) Northeast Arabian Sea [199].

4.5.2. Climate Reconstructions Comparison—Quantitative Approach

The quantitative climate (precipitation and temperature) reconstructions developed in the present study were compared graphically with available Late Holocene reconstructions (Figure 12). For this comparison, reconstructed temperature and precipitation data using other proxy data were procured from NOAA data contributors and also provided by the author of the research paper.

The MAP reconstruction is compared with available precipitation, drought, and ice core records. The MAP is compared with 3500 years of annual precipitation reconstruction from the Northeastern Tibetan Plateau based on tree-ring data [205] and the north central China 1800-year decadal precipitation index reconstruction using stalagmite and historical document records [206] shows similar trends in the later period of MWP and LIA. The reconstructed Palmer drought severity index (PDSI) from the Monsoon Asia Drought Atlas (MADA) [207] from the nearest grid point (88.75/28.75) in the present study site also shows consistency in the trends during LIA. The MAP has been also compared with ice core records of Rongbuk Glacier [173], Dasuopu [208,209], Guliya [210], Dunde [211], and Puruogangri core I and II [212]. Apart from Puruogangri core II, all other ice core records compared with the present reconstructed MAP shows similar variability in the reconstruction.

Similarly, the present reconstructed temperature (MAT) has been compared with temperature reconstructions from adjoining areas and regional, Arctic, hemispheric and global records (Figure 13). The tree-ring-based June–August temperature reconstruction from Bhutan [16] shows cold conditions during the early 15th, 16th, and late 17th to early 18th centuries. Another tree-ring-based temperature reconstruction from Nepal [200] also shows a lowering of temperature during AD 1670–1770, which falls in the period of LIA. In addition, temperature reconstruction for Asia [213] using multi-proxy records, temperature reconstruction using stalagmite records from Beijing, China [214], temperature reconstruction in China using proxy records with methods of principal component regression and partial least squares regression [215], and Arctic-wide temperature reconstruction for the past 2000 years [216] also show comparable variability with the present reconstructed temperature. The temperature reconstructions available from various hemispheric and global levels include: multi-proxy reconstructions of the extra-tropical northern hemisphere (30–90° N) mean temperature [217]; reconstructions of northern hemisphere temperatures and climate forcing over the past 1000 years using multi-proxy records [218]; low-frequency temperature signals reconstructed using Regional Curve Standardized tree-ring chronologies from 14 sites in the northern hemisphere extra-tropics [219]; northern hemisphere high-elevation tree-ring-based temperature reconstruction using the regional curve standardization technique [220]; multi-proxy northern hemisphere temperature reconstruction using inverse regression-truncated EOF climate field reconstruction [221]; northern hemisphere temperature reconstruction calculated by combining low-resolution proxies with tree-ring data [222]; multi-proxy northern hemispheric surface temperature reconstruction [223]; and multi proxy global surface temperature [224] also show similar temperature variability to the present temperature reconstruction in different time periods, especially

during MWP and LIA (Figure 13). However, the differences in variability in both the temperature and precipitation comparative analysis with the present climate reconstruction might be due to the differences in the proxy data used, the reconstructed seasons, and the resolution of the proxies.

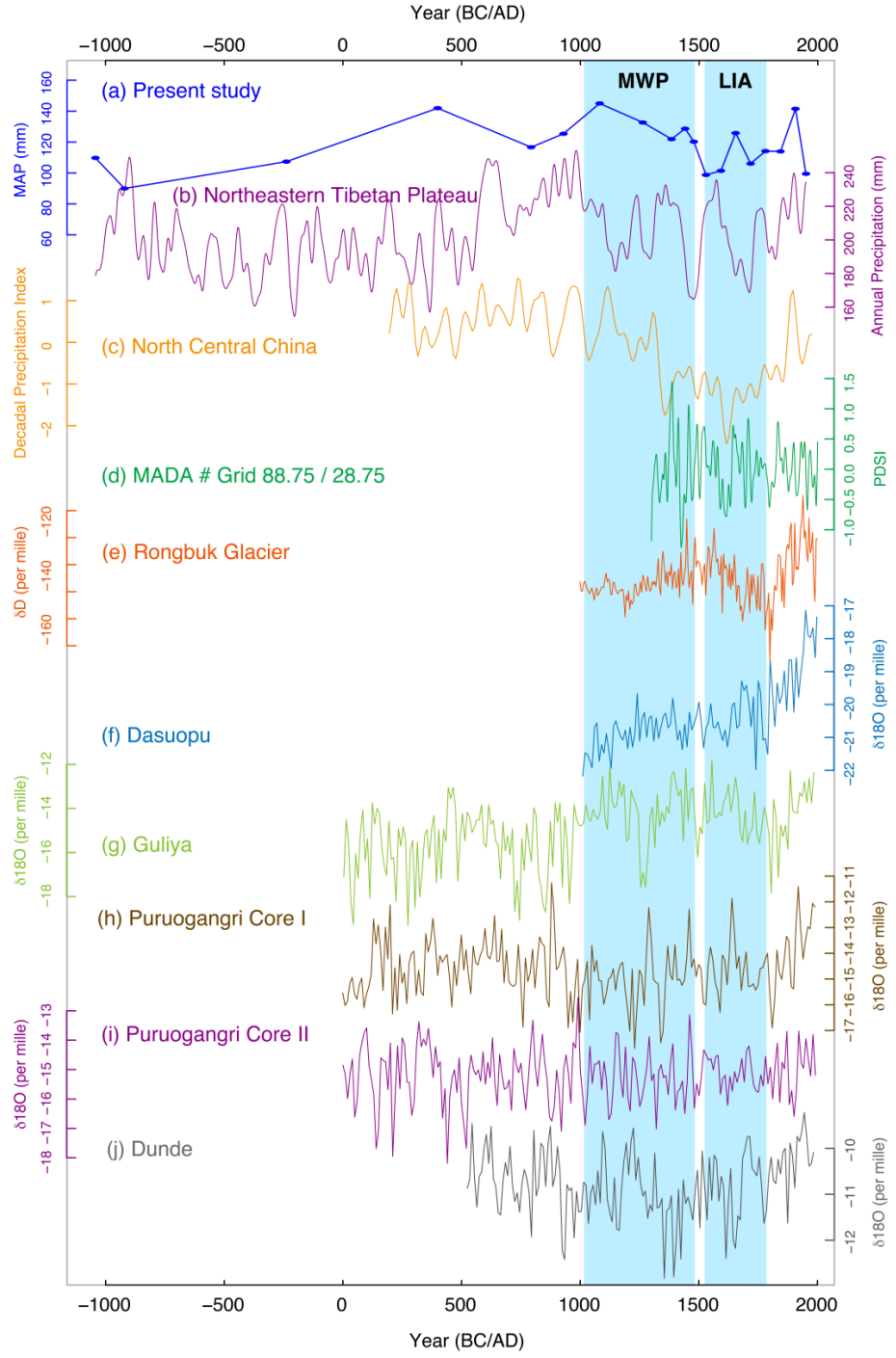

Figure 12. Comparison of (**a**) reconstructed MAP (present study) with other proxy-based climate reconstruction (**b**) annual precipitation from northeastern Tibetan Plateau [205], (**c**) decadal precipitation index from northcentral China [206], (**d**) PDSI from Monsoon Asian Drought Atlas (MADA) [207], (**e**) ice core record from Rongbuk glacier, Nepal [173], (**f**) ice core record from Dasuopu [208,209], (**g**) ice core record from Guliya, Tibetan Plateau [210], (**h**,**i**) ice core record from Puruogangri core I and II [212] and (**j**) ice core record from Dunde [211].

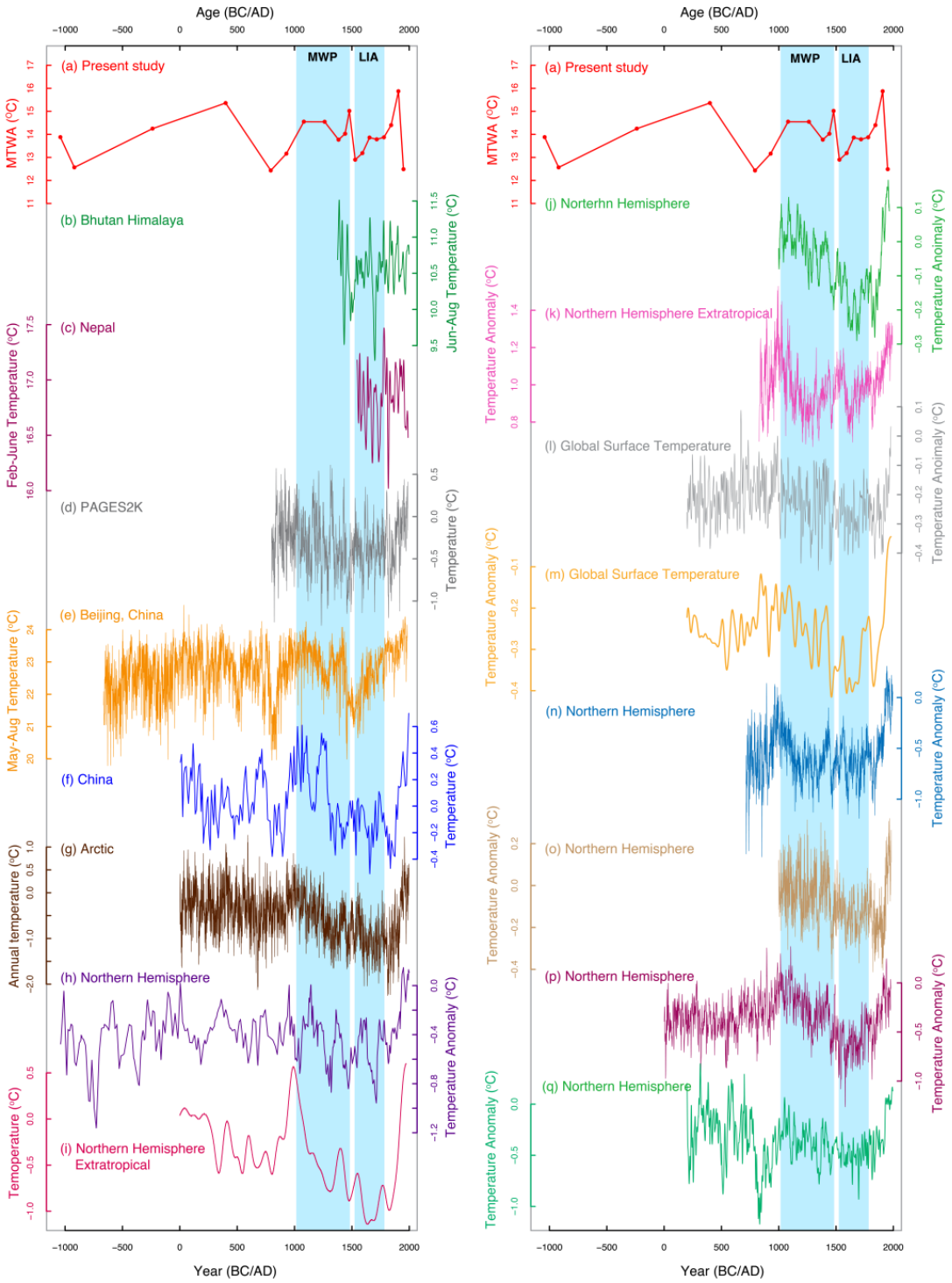

Figure 13. Comparison of (**a**) reconstructed MTWA (present study) with other proxy-based temperature reconstructions (**b**) summer temperature from Bhutanese Himalaya [16], (**c**) February-June temperature from Nepal [200], (**d**) Pages 2k Consortium temperature reconstruction [213], (**e**) stalagmite based warm season temperature from Beijing, China [214] (**f**) temperature reconstruction from China [215], (**g**) temperature reconstruction from Arctic [216], (**h**) extra-tropical Northern Hemisphere temperature reconstruction [217], (**i**) Northern Hemisphere temperature reconstruction [218], (**j**) Northern Hemisphere temperature reconstruction [219] (**k**) extra-tropical Northern Hemisphere temperature reconstruction [220] (**l**) global surface temperature reconstruction [221] (**m**) global surface temperature reconstruction [222] (**n**–**p**) Northern Hemisphere temperature reconstruction [223] (**q**) Northern Hemisphere temperature reconstruction [224].

4.6. Climate Reconstructions and Fluctuation of Sikkimese Glaciers

The present findings of LIA in the climate reconstructions might have linkages with the advances and retreats of the Zemu glacier and other glaciers in Sikkim, Himalaya. In 1995, a study team at the Khangchendzonga Biosphere Reserve reported that since the LIA, the Zemu glacier, Onglokthang glacier, and Rathong Chu glacier in North Sikkim had retreated by 3–4 km, ~500 m, and ~600 m, respectively [225]. A similar response of the cold and dry period of climate on glacier advancement has been recorded in the glacier region of Sithikher Bog, western Himalayas [179], and the Sonapani glacier advance stage II in the Lahaul valley, western Himalayas [226]. The climate reconstruction from this largest glacier of the eastern Himalayas also shows consistency with the climatic observations of the Late Holocene made from the other largest glacier of the western Himalayas [177]. Chaujar [186] also reported that the northern and southern hemispheric glaciers started their retreat in the mid-18th century, which indicates the end of the LIA climatic period. This temporal linkage suggests the possible existence of a common trend in the mountain regions of both hemispheres and the Himalayas, and, thus, its occurrence is a global phenomenon.

Observations made during the early 1940s and 1970s [106,227,228] also suggested the expansion and then receding of the Zemu glacier. The valley has its maximum depth at the center, where the thickness of the glacier ice exceeds 300 m. This suggests that the glacier once occupied the entire valley, extending from the northern to the southern rock walls, and that it has undergone considerable lateral shrinkage, giving rise to the northern and southern trenches. Subsequent movement of the glacier, confined by the lateral moraine ridges, has eroded the bedrock to a greater extent in the central zone than that underlying the trenches from which the glacier has receded to its present position [106].

The Zemu Glacier, located in in Sikkim, the Himalayas, which was visited by the 2nd German Himalaya Expedition in 1931, has been receding since 1891 [227,228], which correlates with evidence from our records of warming trends in temperature. These observations support the evidence of LIA-like events and recent warming phases recorded in our quantitative temperature reconstruction.

The climate oscillation recorded in the present climate reconstruction, especially during the well-known global climate periods of MWP (warm–humid climate) and LIA (cold–dry climate), could be related to glacier behavior and tree line fluctuations. During the warm and humid period, the glaciers might have retreated in this region, and, as a consequence, tree line might ascend to higher elevations. During the cold–dry period, the glacier of this region as well as the tree line might have advanced towards the lower elevations. Thus, the pollen-based climate reconstruction from the glacier region enabled a chronology of glacier activity for the LIA and more recent periods to be established.

The model simulations support the suggestion that the LIA may have been brought about by low northern hemisphere orbital forcing during the Late Holocene, with coincidentally unusually low solar activity and a high number of major volcanic events [162]. So, we can contemplate that this region of the Himalaya was also influenced by solar fluctuations and volcanic activities that occurred elsewhere during the LIA period. The tree-ring studies carried out in the adjacent Bhutan Himalaya [16] also reported that the cooling of the climate during LIA was influenced by solar and volcanic eruptions.

5. Conclusions

The calibration set for modern pollen–climate (temperature and precipitation) provided the development of quantitative climate reconstructions from sub-surface sediment pollen spectra from the Zemu glacier region, eastern Himalayas. The development of a transfer function model using a linear model based on Partial Least Square regression led to the reconstruction of the mean annual precipitation (MAP) and the mean temperature of the warmest month (MTWA). Precipitation has the strongest influence on the composition of the modern pollen samples among the other climatic variables considered in the analysis. The climate reconstruction based on pollen data, supplemented with environmental magnetism analysis, cumulatively indicates the changing climatic scenario around the Zemu

Glacier during the later part of the Holocene. In the absence of long-term instrumental records from this largest glacier region of the eastern Himalayas, proxy-based quantitative climate reconstructions provide an understanding of the relative contribution of changes in temperature and precipitation in glacier environments. The present study provided valuable insight into past precipitation and temperature changes, which helped us identify shifts in climatic conditions as demonstrated by various research outputs, from regional to hemispheric. The climatic variability reconstructed in this study clearly demonstrates close agreement between oscillatory climatic phenomena of the past in the region of the North Atlantic Ocean and the distant Himalayas. Our climate reconstructions capture well-documented world-wide climatic events, such as the MWP and LIA, as well as those of the even earlier Dark Ages Cold Period and Roman Warm Period. Since the present climate reconstructions have been carried out at a remote location in the largest glaciated region of the eastern Himalayas, the observed warming during the late 19th century and then the cooling trend during the early 20th century are most likely of natural origin and not due to any anthropogenic influences. The overall assessment of quantitative climate reconstruction in the Zemu glacier area and its temporal trends, which are comparable with regional, continental, hemispheric perspectives and from a global perspective, should look forward to a more comprehensive analysis with both spatial and temporal coverage.

Supplementary Materials: The following supporting information can be downloaded at: https://www.mdpi.com/article/10.3390/quat6020032/s1, Supplementary Material. Additional details of Material and methods, results and discussions along with Table S1: Sampling site details.

Author Contributions: Conceptualization, N.M. and S.K.S.; methodology, N.M. and S.K.S.; software, N.M. and S.K.S.; validation, N.M., S.K.S. and N.B.; formal analysis, N.M.; investigation, N.M.; resources, N.M., S.K.S. and N.B.; data curation, N.M., S.K.S. and N.B.; writing—original draft preparation, N.M. and S.K.S.; writing—review and editing, N.M., S.K.S. and N.B.; visualization, S.K.S.; supervision, S.K.S. and N.B.; project administration, S.K.S.; funding acquisition, N.M. All authors have read and agreed to the published version of the manuscript.

Funding: This research was funded by Department of Science and Technology (DST), New Delhi, India, grant number ESS–91/38/2005 and DST-WOS(A) scheme for the project No. SR/WOS-A/ES-18/2014(G).

Data Availability Statement: The data that support the findings of this study are available from the corresponding author upon request.

Acknowledgments: The authors (NM and SKS) are thankful to the Director, Birbal Sahni Institute of Palaeosciences, Lucknow for providing the necessary support and facilities to them for the compilation and to publish this work (BSIP No. 11/2015-16). Thanks, are also due to Late R. Ramesh, Physical Research Laboratory, Ahmadabad for providing us C–14 dates of the sediments. The author (NM) is grateful to the Indian Institute of Geomagnetism, Navi Mumbai, India for providing her permission and facilities to work on environmental geomagnetism. Author (SKS) is thankful to Pradeep Kumar, CCF and Usha Lachungpa, Principal Research Officer (WL) from Department of Forest, Government of Sikkim for providing all the support and permission to carry out the field work in North Sikkim. Authors are also thankful to NOAA for providing contributed climate reconstruction data. One of the authors NM is highly grateful to the C.S.I.R., Government of India for providing her financial support during the period of her PhD dissertation. Author NM is also grateful to Department of Science and Technology (DST), New Delhi for the financial support provided to her during the compilation of this manuscript, under the WOS(A) scheme for the project No. SR/WOS-A/ES-18/2014(G). Author SKS also wish to thanks porters especially Tshering Lachenpa and Pema Lachenpa who helped him during the field expedition to this high-altitude glacier terrain of the North Sikkim. The authors are indebted to three anonymous reviewers for their critical comments and valuable suggestions.

Conflicts of Interest: The authors declare no conflict of interest.

References

1. Sarntheina, M.; Kennett, J.P.; Allen, J.R.M.; Beer, J.; Grootes, P.; Laj, C.; McManus, J.; Ramesh, R.; SCOR—IMAGES Working Group 117. Decadal–to–millennial–scale climate variability—Chronology and mechanisms: Summary and recommendations. *Quat. Sci. Rev.* **2002**, *21*, 1121–1128. [CrossRef]
2. Bradley, R.S. Past global changes and their significance for the future. *Quat. Sci. Rev.* **2000**, *19*, 391–402. [CrossRef]
3. Beniston, M. Climate Change in Mountain Regions: A Review of Possible Impacts. *Clim. Chang.* **2003**, *59*, 5–31. [CrossRef]
4. Whiteman, D. *Mountain Meteorology*; Oxford University Press: New York, NY, USA, 2000; p. 355.
5. Thompson, L.G. Ice core evidence for climate changes in the Tropics: Implications for our future. *Quat. Sci. Rev.* **2000**, *19*, 19–35. [CrossRef]
6. Lowe, J.J.; Walker, M.J.C. *Reconstructing Quaternary Environments*, 2nd ed.; Longman Asia Limited: Hong Kong, China, 2015.
7. Bradley, R.S. *Paleoclimatology: Reconstructing Climates of the Quaternary*, 3rd ed.; Elsevier/Academic Press: San Diego, CA, USA, 2014; p. 675.
8. Lamb, H. The early medieval warm epoch and its sequel. *Palaeogeogr. Palaeoclim. Palaeoecol.* **1965**, *1*, 13–37. [CrossRef]
9. Stine, S. Medieval climatic anomaly in the Americas. In *Water, Environment and Society in Times of Climatic Change*; Issar, A.S., Brown, N., Eds.; Kluwer: Dordrecht, The Netherlands, 1998; pp. 43–67.
10. Mann, M.E.; Zhang, Z.; Rutherford, S.; Bradley, R.S.; Hughes, M.K.; Shindell, D.; Ammann, C.; Faluvegi, G.; Ni, F. Global signatures and dynamical origins of the little ice age and Wanner medieval climate anomaly. *Science* **2009**, *326*, 1256–1260. [CrossRef] [PubMed]
11. Graham, N.E.; Ammann, C.M.; Fleitmann, D.; Cobb, K.M.; Luterbacher, J. Support for global climate reorganization during the "Medieval Climate Anomaly". *Clim. Dyn.* **2010**, *37*, 1217–1245. [CrossRef]
12. Grove, J.M. *The Little Ice Age*; Methuen: London, UK, 1988.
13. Bhattacharyya, A.; Shah, S.K. Tree–ring study in India—Past appraisal, present status and future prospects. *IAWA* **2009**, *30*, 361–370. [CrossRef]
14. Bhattacharyya, A.; Chaudhary, V. Late-Summer Temperature Reconstruction of the Eastern Himalayan Region Based on Tree-Ring Data of Abies densa. *Arct. Antarct. Alp. Res.* **2003**, *35*, 196–202. [CrossRef]
15. Shah, S.K.; Mehrotra, N.; Bhattacharyya, A. Tree ring studies from Eastern Himalaya: Prospects and challenges. *Him. Res. J.* **2014**, *2*, 21–28.
16. Krusic, P.J.; Cook, E.R.; Dukpa, D.; Putnam, A.E.; Rupper, S.; Schaefer, J. Six hundred thirty-eight years of summer temperature variability over the Bhutanese Himalaya. *Geophys. Res. Lett.* **2015**, *42*, 2988–2994. [CrossRef]
17. Birks, H.J.B. The use of pollen analysis in the reconstruction of past climates: A review. In *Climate and History*; Wigley, T.M.L., Ingram, M.J., Farmer, G., Eds.; Cambridge University Press: Cambridge, UK, 1981; pp. 111–138.
18. Huntley, B. Quaternary palaeoecology and ecology. *Quat. Sci. Rev.* **1996**, *15*, 591–606. [CrossRef]
19. Birks, H.J.B. Numerical analysis methods. In *Encyclopedia of Quaternary Science*; Elias, S., Ed.; Elsevier: Amsterdam, The Netherlands, 2007; pp. 2514–2521.
20. Brewer, S.; Guiot, J.; Barboni, D. Use of pollen as climate proxies. In *Encyclopedia of Quaternary Science*; Elias, S., Ed.; Elsevier: Amsterdam, The Netherlands, 2007; pp. 2497–2508.
21. Edwards, M.E. BIOME model of vegetation reconstruction. In *Encyclopedia of Quaternary Science*; Elias, S., Ed.; Elsevier: Amsterdam, The Netherlands, 2007; pp. 2551–2561.
22. Seppä, H. Pollen analysis, Principles. In *Encyclopedia of Quaternary Science*; Elias, S., Ed.; Elsevier: Amsterdam, The Netherlands, 2007; pp. 2486–2497.
23. Bhattacharyya, A.; Ranhotra, P.S.; Shah, S.K. Temporal and spatial variations of late Pleistocene–Holocene climate of the western Himalaya based on pollen records and their implications to Monsoon dynamics. *J. Geol. Soc. India* **2006**, *68*, 507–515.
24. Bhattacharyya, A.; Ranhotra, P.S.; Shah, S.K. Spatio Temporal Variation of Alpine Vegetation vis–à–vis Climate during Holocene in the Himalaya. *Mem. Geol. Soc. India* **2011**, *77*, 309–319.
25. Mehrotra, N.; Shah, S.K.; Bhattacharyya, A. Review of palaeoclimate records from Northeast India based on pollen proxy data of Late Pleistocene–Holocene. *Quat. Int.* **2014**, *325*, 41–54. [CrossRef]
26. Seppä, H.; Bennett, K.D. Quaternary pollen analysis: Recent progress in palaeoecology and palaeoclimatology. *Prog. Phys. Geogr.* **2003**, *27*, 548–579. [CrossRef]
27. Iversen, J. Viscum, Hedera and Ilex as climatic indicators. A contribution to the study of the post–glacial temperature climate. *Geol. Föreningens I Stockh. Förhandlingar* **1944**, *66*, 463–483. [CrossRef]
28. Grichuk, V.P. An experiment in reconstructing some characteristics of climate in the Northern Hemisphere during the Atlantic Period of Holocene. In *Holocene*; Neustadt, M.I., Ed.; Nauka: Moscow, Russia, 1969; pp. 41–57.
29. Tarasov, P.E.; Nakagawa, T.; Demske, D.; Österle, H.; Igarashi, Y.; Kitagawa, J.; Mokhova, L.; Bazarova, V.; Okuda, M.; Gotanda, K.; et al. Progress in the reconstruction of Quaternary climate dynamics in the Northwest Pacific: A new modern analogue reference dataset and its application to the 430-kyr pollen record from Lake Biwa. *Earth Sci. Rev.* **2011**, *108*, 64–79. [CrossRef]
30. Imbrie, J.; Kipp, N.G. A new micropaleontological method for quantitative paleoclimatology: Application to a late Pleistocene Caribbean core. In *The Late Cenozoic Glacial Ages*; Turekian, K.K., Ed.; Yale University Press: New Haven, CT, USA, 1971; pp. 71–181.

31. Webb, I.I.I.T.; Thompson, B.; Bryson, R.A. Late-and postglacical climatic change in the northern Midwest, USA: Quantitative estimates from fossil pollen spectra by multivariate statistical analysis. *Quat. Res.* **1972**, *2*, 70–115. [CrossRef]
32. Bartlein, P.J.; Webb, T.I.I.I.; Fleri, E. Holocene climatic change in the northern Midwest: Pollen–derived estimates. *Quat. Res.* **1984**, *22*, 361–374. [CrossRef]
33. Bartlein, P.J.; Webb, T.I.I.I. Mean July temperature at 6000 yr B.P. in eastern North America: Regression equations for estimates from fossil–pollen data. *Syllogeus* **1985**, *55*, 301–342.
34. Guiot, J. Late Quaternary Climatic Change in France Estimated from Multivariate Pollen Time Series. *Quat. Res.* **1987**, *28*, 100–118. [CrossRef]
35. Huntley, B.; Prentice, I.C. July temperature in Europe from pollen data, 6000 years before present. *Science* **1988**, *241*, 687–690. [CrossRef]
36. Guiot, J.; Pons, A.; de Beaulieu, J.-L.; Reille, M. A 140,000–year climatic reconstruction from two European pollen records. *Nature* **1989**, *338*, 309–313. [CrossRef]
37. ter Braak, C.J.F.; Juggins, S. Weighted averaging partial least squares regression (WA–PLS): An improved method for reconstruction environmental variables from species assemblages. *Hydrobiologia* **1993**, *269*, 485–502. [CrossRef]
38. Birks, H.J.B. Quantitative palaeoenvironmental reconstructions. In *Statistical Modelling of Quaternary Science Data*; Maddy, D., Brew, J.S., Eds.; Quaternary Research Association: Cambridge, UK, 1995; pp. 161–254.
39. Peyron, O.; Guiot, J.; Cheddadi, R.; Tarasov, P.E.; Reille, M.; deBeaulieu, J.-L.; Bottema, S.; Andrieu, V. Climatic reconstruction in Europe from pollen data, 18,000 years before present. *Quat. Res.* **1998**, *49*, 183–196. [CrossRef]
40. Seppä, H.; Birks, H.J.B. July mean temperature and annual precipitation trends during the Holocene in the Fennoscandian tree–line area, pollen–based reconstructions. *Holocene* **2001**, *11*, 527–539. [CrossRef]
41. Seppä, H.; Birks, H. Holocene Climate Reconstructions from the Fennoscandian Tree-Line Area Based on Pollen Data from Toskaljavri. *Quat. Res.* **2002**, *57*, 191–199. [CrossRef]
42. Markgraf, V.; Webb, R.S.; Anderson, K.H.; Anderson, L. Modern pollen/climate calibration for southern South America. Palaeogeogr. *Palaeoclimatol. Palaeoecol.* **2002**, *181*, 375–397. [CrossRef]
43. Davis, B.; Brewer, S.; Stevenson, A.; Guiot, J. The temperature of Europe during the Holocene reconstructed from pollen data. *Quat. Sci. Rev.* **2003**, *22*, 1701–1716. [CrossRef]
44. Seppä, H.; Birks, H.J.B.; Odland, A.; Poska, A.; Veski, S. A modern pollen-climate calibration set from northern Europe: Developing and testing a tool for palaeoclimatological reconstructions. *J. Biogeogr.* **2004**, *31*, 251–267. [CrossRef]
45. Seppä, H.; Hammarlund, D.; Antonsson, K. Low–frequency and high frequency changes in temperature and effective humidity during the Holocene in south–central Sweden, implications for atmospheric and oceanic forcings of climate. *Clim. Dyn.* **2005**, *25*, 285–297. [CrossRef]
46. Seppä, H.; MacDonald, G.M.; Birks, H.J.B.; Gervais, B.R.; Snyder, J.A. Late-Quaternary summer temperature changes in the northern-European tree-line region. *Quat. Res.* **2008**, *69*, 404–412. [CrossRef]
47. Seppä, H.; Bjune, A.E.; Telford, R.J.; Birks, H.J.B.; Veski, S. Last nine-thousand years of temperature variability in Northern Europe. *Clim. Past* **2009**, *5*, 523–535. [CrossRef]
48. Tarasov, P.; Granoszewski, W.; Bezrukova, E.; Brewer, S.; Nita, M.; Abzaeva, A.; Oberhänsli, H. Quantitative reconstruction of the last interglacial vegetation and climate based on the pollen record from Lake Baikal, Russia. *Clim. Dyn.* **2005**, *25*, 625–637. [CrossRef]
49. Tarasov, P.E.; Bezrukova, E.V.; Krivonogov, S.K. Late glacial and Holocene changes in vegetation cover and climate in southern Siberia derived from a 15 kyr long pollen record from Lake Kotokel. *Clim. Past.* **2009**, *5*, 73–84. [CrossRef]
50. Peros, M.C.; Gajewski, K. Holocene climate and vegetation change on Victoria Island, western Canadian Arctic. *Quat. Sci. Rev.* **2008**, *27*, 235–249. [CrossRef]
51. Dormoy, I.; Peyron, O.; Nebout, N.C.; Goring, S.; Kotthoff, U.; Magny, M.; Pross, J. Terrestrial climate variability and seasonality changes in the Mediterranean region between 15 000 and 4000 years BP deduced from marine pollen records. *Clim. Past* **2009**, *5*, 615–632. [CrossRef]
52. Litt, T.; Schölzel, C.; Kühl, N.; Brauer, A. Vegetation and climate history in the Westeifel Volcanic Field (Germany) during the past 11 000 years based on annually laminated lacustrine maar sediments. *Boreas* **2009**, *38*, 679–690. [CrossRef]
53. Bartlein, P.J.; Harrison, S.; Brewer, S.; Connor, S.; Davis, B.A.S.; Gajewski, K.; Guiot, J.; Harrison-Prentice, T.I.; Henderson, A.P.; Peyron, O.; et al. Pollen-based continental climate reconstructions at 6 and 21 ka: A global synthesis. *Clim. Dyn.* **2011**, *37*, 775–802. [CrossRef]
54. Nakagawa, T.; Tarasov, P.E.; Nishida, K.; Gotanda, K.; Yasuda, Y. Quantitative pollen-based climate reconstruction in central Japan: Application to surface and Late Quaternary spectra. *Quat. Sci. Rev.* **2002**, *21*, 2099–2113. [CrossRef]
55. Nakagawa, T.; Kitagawa, H.; Yasuda, Y.; Tarasov, P.E.; Kotoba, N.; Gotanda, K.; Sawai, Y.; Program, Yangtze River Civilization. Asynchronous Climate Changes in the North Atlantic and Japan During the Last Termination. *Science* **2003**, *299*, 688–691. [CrossRef] [PubMed]
56. Jiang, W.; Guo, Z.; Sun, X.; Wu, H.; Chu, G.; Yuan, B.; Hatté, C.; Guiot, J. Reconstruction of climate and vegetation changes of Lake Bayanchagan (Inner Mongolia): Holocene variability of the East Asian monsoon. *Quat. Res.* **2006**, *65*, 411–420. [CrossRef]
57. Shen, C.; Liu, K.-B.; Tang, L.; Overpeck, J.T. Quantitative relationships between modern pollen rain and climate in the Tibetan Plateau. *Rev. Palaeobot. Palynol.* **2006**, *140*, 61–77. [CrossRef]

58. Tarasov, P.; Jin, G.; Wagner, M. Mid-Holocene environmental and human dynamics in northeastern China reconstructed from pollen and archaeological data. *Palaeogeogr. Palaeoclim. Palaeoecol.* **2006**, *241*, 284–300. [CrossRef]
59. Li, Y.; Xu, Q.; Liu, J.; Yang, X.; Nakagawa, T. A transfer-function model developed from an extensive surface-pollen data set in northern China and its potential for palaeoclimate reconstructions. *Holocene* **2007**, *17*, 897–905. [CrossRef]
60. Zhu, C.; Chen, X.; Zhang, G.S.; Ma, C.M.; Zhu, Q.; Li, Z.X.; Xu, W.F. Spore pollen–climate factor transfer function and paleoenvironment reconstruction in Dajiuhu, Shennongjia, Central China. *Chin. Sci. Bull.* **2008**, *53*, 42–49. [CrossRef]
61. Herzschuh, U.; Kramer, A.; Mischke, S.; Zhang, C. Quantitative climate and vegetation trends since the late glacial on the northeastern Tibetan Plateau deduced from Koucha Lake pollen record. *Quat. Res.* **2009**, *71*, 162–171. [CrossRef]
62. Herzschuh, U.; Birks, H.J.B.; Mischke, S.; Zhang, C.; Böhner, J. A modern pollen-climate calibration set based on lake sediments from the Tibetan Plateau and its application to a Late Quaternary pollen record from the Qilian Mountains. *J. Biogeogr.* **2010**, *37*, 752–766. [CrossRef]
63. Xu, Q.; Xiao, J.; Li, Y.; Tian, F.; Nakagawa, T. Pollen–Based Quantitative Reconstruction of Holocene Climate Changes in the Daihai Lake Area, Inner Mongolia, China. *J. Clim.* **2010**, *23*, 2856–2867. [CrossRef]
64. Park, J. A modern pollen–temperature calibration data set from Korea and quantitative temperature reconstructions for the Holocene. *Holocene* **2011**, *21*, 1125–1135. [CrossRef]
65. Sun, A.; Feng, Z. Holocene climatic reconstructions from the fossil pollen record at Qigai Nuur in the southern Mongolian Plateau. *Holocene* **2013**, *23*, 1391–1402. [CrossRef]
66. Wen, R.; Xiao, J.; Ma, Y.; Feng, Z.; Li, Y.; Xu, Q. Pollen–climate transfer functions intended for temperate eastern Asia. *Quat. Int.* **2013**, *311*, 3–11. [CrossRef]
67. Birks, H.J.B. Numerical tools in palaeolimnology—Progress, potentialities, and problems. *J. Paleolimnol.* **1998**, *20*, 307–332. [CrossRef]
68. Birks, H.J.B.; Seppä, H. Pollen–based reconstructionsof late–Quaternary climate in Europe—Progress, problems, and pitfalls. *Acta Palaeobot.* **2004**, *44*, 317–334.
69. Kumke, T.; Schölzel, C.; Hense, A. Transfer functions for palaeoclimate reconstructions—Theory and methods. In *The Climate in Historical Times*; Fischer, H., Kumke, T., Lohmann, G., Flöser, G., Miller, H., von Storch, H., Negendank, J.F.W., Eds.; Springer: Berlin, Germany, 2004; pp. 229–243.
70. John, H.; Birks, B. Quantitative palaeoenvironmental reconstructions from Holocene Biological data. In *Global Change in the Holocene*; Mackay, A., Rick, B., Birks, J., Oldfield, F., Eds.; Arnold: London, UK, 2005; p. 528.
71. Telford, R.; Birks, H. The secret assumption of transfer functions: Problems with spatial autocorrelation in evaluating model performance. *Quat. Sci. Rev.* **2005**, *24*, 2173–2179. [CrossRef]
72. Guiot, J.; de Vernal, A. Transfer functions: Methods for quantitative paleoceanography based on microfossils. In *Developments in Marine Geology 1—Proxies in Late Cenozoic Paleoceanography*; Hillaire Marcel, C., de Vernal, A., Eds.; Elsevier: Amsterdam, Netherlands, 2007; pp. 523–563.
73. Guiot, J. Transfer Functions. *IOP Conf. Ser. Earth Environ. Sci.* **2011**, *14*, 1–6. [CrossRef]
74. Juggins, S.; Birks, H.J.B. Quantitative environmental reconstructions from biostratigraphical data. In *Tracking Environmental Change Using Lake Sediments Data Handling and Numerical Techniques*; Birks, H.J.B., Lotter, A.F., Juggins, S., Smol, J.P., Eds.; Springer: Dordrecht, The Netherlands, 2011; Volume 5.
75. Lu, H.; Wu, N.; Liu, K.-B.; Zhu, L.; Yang, X.; Yao, T.; Wang, L.; Li, Q.; Liu, X.; Shen, C.; et al. Modern pollen distributions in Qinghai–Tibetan Plateau and the development of transfer functions for reconstructing Holocene environmental changes. *Quat. Sci. Rev.* **2011**, *30*, 947–966. [CrossRef]
76. Ohlwein, C.; Wahl, E.R. Review of probabilistic pollen-climate transfer methods. *Quat. Sci. Rev.* **2012**, *31*, 17–29. [CrossRef]
77. Birks, H.J.B. Numerical methods for the analysis of diatom assemblage data. In *The Diatoms—Applications for the Environmental and Earth Sciences*; Smol, J.P., Stoermer, E.F., Eds.; Cambridge University Press: Cambridge, UK, 2010; pp. 23–54.
78. Ghosh, R.; Paruya, D.K.; Khan, M.A.; Chakraborty, S.; Sarkar, A.; Bera, S. Late Quaternary climate variability and vegetation response in Ziro Lake Basin, Eastern Himalaya: A multiproxy approach. *Quat. Int.* **2014**, *325*, 13–29. [CrossRef]
79. Ghosh, R.; Bera, S.; Sarkar, A.; Paruya, D.K.; Yao, Y.F.; Li, C.S. ~50 ka record of monsoonal variability in the Darjeeling foothill region, eastern Himalayas. *Quat. Sci. Rev.* **2015**, *114*, 100–115. [CrossRef]
80. Mosbrugger, V.; Utescher, T. The coexistence approach—A method for quantitative reconstructions of Tertiary terrestrial palaeoclimate data using plant fossils. *Palaeogeogr. Palaeoclim. Palaeoecol.* **1997**, *134*, 61–86. [CrossRef]
81. Utescher, T.; Bruch, A.; Erdei, B.; François, L.; Ivanov, D.; Jacques, F.; Kern, A.; Liu, Y.-S.; Mosbrugger, V.; Spicer, R. The Coexistence Approach—Theoretical background and practical considerations of using plant fossils for climate quantification. *Palaeogeogr. Palaeoclim. Palaeoecol.* **2014**, *410*, 58–73. [CrossRef]
82. Sun, N.; Li, X.Q. The quantitative reconstruction of the palaeoclimate between 5200 and 4300 cal yr BP in the Tianshui Basin, NW China. *Clim. Past* **2012**, *8*, 625–636. [CrossRef]
83. Tang, Y.-N.; Li, X.; Yao, Y.-F.; Ferguson, D.K.; Li, C.-S. Environmental Reconstruction of Tuyoq in the Fifth Century and Its Bearing on Buddhism in Turpan, Xinjiang, China. *PLoS ONE* **2014**, *9*, e86363. [CrossRef] [PubMed]
84. Sharma, C.; Chauhan, M.S. Palaeoclimatic inferences from quaternary palynostratigraphy of the Himalayas. In *The Himalayan Environment*; Dash, S.K., Bahadur, J., Eds.; New Age International: New Delhi, India, 1999; pp. 193–207.

85. Sharma, C.; Chauhan, M.S. Late Holocene vegetation climate Kupup Sikkim, eastern Himalaya, India. *J. Palaeontol. Soc. India* **2001**, *46*, 51–58.
86. Sharma, C.; Chauhan, M.S. Vegetation and climate since Last Glacial Maxima in Darjeeling (Mirik Lake), Eastern Himalaya. In Proceedings of the 29th International Geological Congress, Kyoto, Japan, 24 August–3 September 1992; pp. 279–288.
87. Chauhan, M.S.; Sharma, C. Late Holovene vegetation of Darjeeling (Jore-Pokhari) eastern Himalaya. *Palaeobotanist* **1996**, *45*, 125–129.
88. Dubey, J.; Ghosh, R.; Agrawal, S.; Quamar, M.; Morthekai, P.; Sharma, R.; Sharma, A.; Pandey, P.; Srivastava, V.; Ali, S.N. Characteristics of modern biotic data and their relationship to vegetation of the Alpine zone of Chopta valley, North Sikkim, India: Implications for palaeovegetation reconstruction. *Holocene* **2018**, *28*, 363–376. [CrossRef]
89. Thompson, R.; Oldfield, F. *Environmental Magnetism*; Allen and Unwin Press: London, UK, 1986.
90. Basavaiah, N.; Khadkikar, A.S. Environmental magnetism and paleomonsoon. *J. Indian Geophys. Union* **2004**, *8*, 1–77.
91. Basavaiah, N. *Geomagnetism: Solid Earth and Upper Atmosphere Perspectives*; Springer: Dordrecht, The Netherlands, 2011; pp. 291–386.
92. Basavaiah, N.; Seetharamaiah, J.; Appel, E.; Juyal, N.; Prasad, S.; Nageswara Rao, K.; Khadkikar, A.S.; Nowaczyk, N.; Brauer, A. Holocene environmental magnetic records of Indian monsoon fluctuations. In *Holocene Climate Change and Environment*; Kumaran, N., Damodara, P., Eds.; Elsevier: Amsterdam, Netherlands, 2022; pp. 229–247. [CrossRef]
93. Sukumaran, P.; Sant, D.A.; Krishnan, K.; Rangarajan, G.; Basavaiah, N.; Schwenninger, J.-L. Multi-Proxy Records of Late Holocene Flood Events From the Lower Reaches of the Narmada River, Western India. *Front. Earth Sci.* **2021**, *9*, 634354. [CrossRef]
94. Maher, B. The magnetic properties of Quaternary aeolian dusts and sediments, and their palaeoclimatic significance. *Aeolian Res.* **2011**, *3*, 87–144. [CrossRef]
95. Liu, Q.; Roberts, A.P.; Larrasoaña, J.C.; Banerjee, S.K.; Guyodo, Y.; Tauxe, L.; Oldfield, F. Environmental magnetism: Principles and applications. *Rev. Geophys.* **2012**, *50*, RG4002. [CrossRef]
96. Maxbauer, D.P.; Feinberg, J.M.; Fox, D.L. Magnetic mineral assemblages in soils and paleosols as the basis for paleoprecipitation proxies: A review of magnetic methods and challenges. *Earth Sci. Rev.* **2016**, *155*, 28–48. [CrossRef]
97. Basavaiah, N.; Juyal, N.; Pant, R.K.; Yadava, M.G.; Singhvi, A.K.; Appel, E. Late Quaternary climate changes reconstructed from mineral magnetic studies from proglacial lake deposits of Higher Central Himalaya. *J. Indian Geophys.Union* **2004**, *8*, 27–38.
98. Juyal, N.; Pant, R.K.; Basavaiah, N.; Yadava, M.G.; Saini, N.K.; Singhvi, A.K. Climate and seismicity in the Higher Central Himalaya during the last 20 ka: Evidences from Garbyang basin, Uttaranchal. *Palaeogeogr. Palaeoclimatol. Palaeoecol.* **2004**, *213*, 315–330. [CrossRef]
99. Juyal, N.; Pant, R.; Basavaiah, N.; Bhushan, R.; Jain, M.; Saini, N.; Yadava, M.; Singhvi, A. Reconstruction of Last Glacial to early Holocene monsoon variability from relict lake sediments of the Higher Central Himalaya, Uttrakhand, India. *J. Asian Earth Sci.* **2009**, *34*, 437–449. [CrossRef]
100. Bhattacharyya, A.; Mehrotra, N.; Shah, S.K.; Basavaiah, N.; Chaudhary, V.; Singh, I.B. Analysis of vegetation and climate change during Late Pleistocene from Ziro Valley, Arunachal Pradesh, Eastern Himalaya region. *Quat. Sci. Rev.* **2014**, *101*, 111–123. [CrossRef]
101. Mehrotra, N.; Shah, S.K.; Basavaiah, N.; Laskar, A.H.; Yadava, M.G. Resonance of the '4.2ka event' and terminations of global civilizations during the Holocene, in the palaeoclimate records around PT Tso Lake, Eastern Himalaya. *Quat. Int.* **2019**, *507*, 206–216. [CrossRef]
102. Basavaiah, N.; Appel, E.; Lakshmi, B.V.; Deenadayalan, K.; Satyanarayana, K.V.V.; Misra, S.; Juyal, N.; Malik, M.A. Revised magnetostratigraphy and characteristics of the fluviolacustrine sedimentation of the Kashmir basin, India, during Pliocene-Pleistocene. *J. Geophys. Res. Solid Earth* **2010**, *115*, B8. [CrossRef]
103. Basavaiah, N.; Babu, J.M.; Gawali, P.; Kumar, K.N.; Demudu, G.; Prizomwala, S.P.; Hanamgond, P.; Rao, K.N. Late Quaternary environmental and sea level changes from Kolleru Lake, SE India: Inferences from mineral magnetic, geochemical and textural analyses. *Quat. Int.* **2015**, *371*, 197–208. [CrossRef]
104. G.S.I. *Geological and Mineral Resources of Sikkim, Geological Survey of India Miscellaneous Publication No. 30, Part XIX—Sikkim*; Government of India: New Delhi, India, 2012.
105. Kaul, M.K. *Inventory of the Himalayan Glaciers*; Special Publication No. 34; Geological Survey of India, India: Kolkata, India, 1999; 165p.
106. Bose, R.N.; Dutta, N.P.; Lahiri, S.M. Refraction seismic investigation at Zemu glacier, Sikkim. *J. Glaciol.* **1971**, *10*, 113–119. [CrossRef]
107. LaTouche, T.H.D. Notes on certain glaciers in Sikkim. *Rec. Geol. Surv. India* **1910**, *40*, 52–62.
108. Dutt, G.N. *Geological Record of the Rangit Valley Expedition, Sikkim*; Unpub. Report, GSI (F.S. 1954-55); 1955.
109. Zhao, L.; Ping, C.-L.; Yang, D.; Cheng, G.; Ding, Y.; Liu, S. Changes of climate and seasonally frozen ground over the past 30 years in Qinghai–Xizang (Tibetan) Plateau, China. *Glob. Planet. Chang.* **2004**, *43*, 19–31. [CrossRef]
110. Cheng, G.; Wu, T. Responses of permafrost to climate change and their environmental significant, Qinghai-Tibet Plateau. *J. Geophys. Res.* **2007**, *112*, F02S03.
111. Samui, R.P. Rainfall variations along the teesta valley in mountainous slope of sikkim. *Mausam* **1994**, *45*, 165–170. [CrossRef]
112. Srivastava, R.C. Introduction. In *Flora of Sikkim*; Hajra, P.K., Verma, D.M., Eds.; Botanical Survey of India, Government of India: New Delhi, India, 1996; pp. 1–22.

113. Smith, W.W.; Cave, G.H. The vegetation of the Zemu and Llonakh valleys of Sikkim. *Rec. Bot. Surv. India* **1911**, *4*, 141–260.
114. Erdtman, G. *An Introduction to Pollen Analysis*; Read Books Ltd.: Waltham, MA, USA, 1943; 239p.
115. Grimm, E.C. *TILIA and TG View 2.0.2, Springfield IL*; Illinois State Museum: Springfield, IL, USA, 2004.
116. Grimm, E.C. CONISS: A FORTRAN 77 program for stratigraphically constrained cluster analysis by the method of incremental sum of squares. *Comput. Geosci.* **1987**, *13*, 13–35. [CrossRef]
117. Ramsey, C.B. Radiocarbon Calibration and Analysis of Stratigraphy: The OxCal Program. *Radiocarbon* **1995**, *37*, 425–430. [CrossRef]
118. Seetharam, K. Climate change scenario over Gangtok. Letters to the editor. Meteorological center, Gangtok, Indian Me-teorological Department, India. *Mausam* **2008**, *59*, 361–366. [CrossRef]
119. New, M.; Lister, D.; Hulme, M.; Makin, I. A high-resolution data set of surface climate over global land areas. *Clim. Res.* **2002**, *21*, 1–25. [CrossRef]
120. Guiot, J.; Goeury, C. PPPBase, a software for statistical analysis of paleoecological and paleoclimatological data. *Dendrochronologia* **1996**, *14*, 295–300.
121. Birks, H.J.B. Overview of Numerical Methods in Palaeolimnology. In *Tracking Environmental Change Using Lake Sediments. Developments in Paleoenvironmental Research*; Birks, H., Lotter, A., Juggins, S., Smol, J., Eds.; Springer: Dordrecht, The Netherlands, 2012; Volume 5. [CrossRef]
122. Prentice, I. Multidimensional scaling as a research tool in quaternary palynology: A review of theory and methods. *Rev. Palaeobot. Palynol.* **1980**, *31*, 71–104. [CrossRef]
123. ter Braak, C.J.F.; Šmilauer, P. *CANOCO Reference Manual and User's Guide: Software for Ordination, Version 5.0*; Microcomputer Power: Ithaca, NY, USA, 2012; p. 496.
124. ter Braak, C.J.F.; Prentice, I.C. A theory of gradient analysis. *Adv. Ecol. Res.* **1988**, *18*, 271–317.
125. Lu, H.Y.; Wu, N.Q.; Yang, X.D.; Jiang, H.; Liu, K.-B.; Liu, T.S. Phytoliths as quantitative indicators for the reconstruction of past environmental conditions in China I: Phytolith–based transfer functions. *Quat. Sci. Rev.* **2006**, *25*, 945–959. [CrossRef]
126. ter Braak, C.J.F. Ordination. In *Data Analysis in Community and Landscape Ecology*; Jongman, R.H., Ter Braak, C.J.F., van Tongeren, O.F.R., Eds.; Pudoc: Wageningen, The Netherlands, 1987; pp. 91–173.
127. ter Braak, C.J.F.; Juggins, S.; Birks, H.J.B.; van der Voet, H. Weighted averaging partial least squares regression (WA-PLS): Definition and comparison with other methods for species-environment calibration. In *Multivariate Environmental Statistics*; Patil, G.P., Rao, C.R., Eds.; Elsevier Science Publishers, B.V.: Amsterdam; The Netherlands, 1993; Chapter 25; pp. 525–560.
128. Wold, S.; Esbensen, K.; Geladi, P. Principal Component Analysis. *Chemom. Intell. Lab. Syst.* **1987**, *2*, 37–52. [CrossRef]
129. Michaelsen, J. Cross-Validation in Statistical Climate Forecast Models. *J. Clim. Appl. Meteorol.* **1987**, *26*, 1589–1600. [CrossRef]
130. R Core Team. R: A Language and Environment for Statistical Computing. R Foundation for Statistical Computing, Vienna, Austria. 2015. Available online: http://www.R--project.org/ (accessed on 28 August 2021).
131. Juggins, S. Rioja: Analysis of Quaternary Science Data, R Package Version (0.8 7). 2012. Available online: http://cran.r--project.org/package=rioja (accessed on 28 August 2021).
132. Beniston, M. *Environmental Changes in Mountains and Uplands*; Arnold Publisher, London and Oxford University Press: New York, NY, USA, 2000; p. 172.
133. Rohli, R.V.; Vega, A.J. *Climatology, Climatology*, 2nd ed.; Jones and Bartlett Learning: Sudbury, MA, USA, 2012; p. 443.
134. Wei, H.-C.; Ma, H.-Z.; Zheng, Z.; Pan, A.-D.; Huang, K.-Y. Modern pollen assemblages of surface samples and their relationships to vegetation and climate in the northeastern Qinghai-Tibetan Plateau, China. *Rev. Palaeobot. Palynol.* **2011**, *163*, 237–246. [CrossRef]
135. Xiao, X.; Shen, J.; Wang, S. Spatial variation of modern pollen from surface lake sediments in Yunnan and southwestern Sichuan Province, China. *Rev. Palaeobot. Palynol.* **2011**, *165*, 224–234. [CrossRef]
136. Luo, C.X.; Zheng, Z.; Tarasov, P.; Nakagawa, T.; Pan, A.D.; Xu, Q.H.; Lu, H.Y.; Huang, K.Y. A potential of pollen–based climate reconstruction using a modern polleneclimate dataset from arid northern and western China. *Rev. Palaeobot. Palynol.* **2010**, *160*, 111–125. [CrossRef]
137. Cao, X.-Y.; Herzschuh, U.; Telford, R.J.; Ni, J. A modern pollen–climate dataset from China and Mongolia: Assessing its potential for climate reconstruction. *Rev. Palaeobot. Palynol.* **2014**, *211*, 87–96. [CrossRef]
138. Maher, B.A.; Thompson, R. Mineral magnetic record of the Chinese loess and paleosols. *Geology* **1991**, *19*, 3–6. [CrossRef]
139. Geiss, C.E.; Egli, R.; Zanner, C.W. Direct estimates of pedogenicmagnetite as a tool to reconstruct past climates from buried soils. *J. Geophys. Res.* **2008**, *113*, B11102. [CrossRef]
140. Balsam, W.L.; Ellwood, B.B.; Ji, J.; Williams, E.R.; Long, X.; El Hassani, A. Magnetic susceptibility as a proxy for rainfall: Worldwide data from tropical and temperate climate. *Quat. Sci. Rev.* **2011**, *30*, 2732–2744. [CrossRef]
141. Orgeira, M.J.; Egli, R.; Compagnucci, R.H. A quantitativemodel of magnetic enhancement in loessic soils. In *The Earth's Magnetic Interior*; Petrovský, E., Ivers, D., Harinarayana, T., Herrero-Bervera, E., Eds.; Springer: Dordrecht, The Netherlands, 2011; pp. 361–397.
142. Hyland, E.G.; Badgley, C.; Abrajevitch, A.; Sheldon, N.D.; Van Der Voo, R. A new paleoprecipitation proxy based on soil magnetic properties: Implications for expanding paleoclimate reconstructions. *GSA Bulletin* **2015**, *127*, 975–981. [CrossRef]
143. Long, X.; Ji, J.; Balsam, W. Rainfall-dependent transformations of iron oxides in a tropical saprolite transect of Hainan Island, South China: Spectral and magnetic measurements. *J. Geophys. Res. Earth Surf.* **2011**, *116*, F3. [CrossRef]

144. Porter, S.C.; Hallet, B.; Wu, X.; An, Z. Dependence of Near-Surface Magnetic Susceptibility on Dust Accumulation Rate and Precipitation on the Chinese Loess Plateau. *Quat. Res.* **2001**, *55*, 271–283. [CrossRef]
145. Ma, M.; Liu, X.; Pillans, B.J.; Hu, S.; Lü, B.; Liu, H. Magnetic properties of Dashing Rocks loess at Timaru, South Island, New Zealand. *Geophys. J. Int.* **2013**, *195*, 75–85. [CrossRef]
146. Begét, J.E.; Stone, D.B.; Hawkins, D.B. Paleoclimatic forcing of magnetic susceptibility variations in Alaskan loess during the late Quaternary. *Geology* **1990**, *18*, 40–43. [CrossRef]
147. Geiss, C.E.; Zanner, C.W.; Banerjee, S.K.; Joanna, M. Signature of magnetic enhancement in a loessic soil in Nebraska, United States of America. *Earth Planet. Sci. Lett.* **2004**, *228*, 355–367. [CrossRef]
148. Geiss, C.E.; Zanner, C.W. How abundant is pedogenic magnetite? Abundance and grain size estimates for loessic soils based on rock magnetic analyses. *J. Geophys. Res. Solid Earth* **2006**, *111*, B12. [CrossRef]
149. Geiss, C.E.; Zanner, C.W. Sediment magnetic signature of climate in modern loessic soils from the Great Plains. *Quat. Int.* **2007**, *162–163*, 97–110. [CrossRef]
150. Maher, B.; Alekseev, A.; Alekseeva, T. Variation of soil magnetism across the Russian steppe: Its significance for use of soil magnetism as a palaeorainfall proxy. *Quat. Sci. Rev.* **2002**, *21*, 1571–1576. [CrossRef]
151. Maher, B.A.; Alekseev, A.; Alekseeva, T. Magnetic mineralogy of soils across the Russian Steppe: Climatic dependence of pedogenicmagnetite formation. *Palaeogeogr. Palaeoclimatol. Palaeoecol.* **2003**, *201*, 321–341. [CrossRef]
152. Maher, B.; Thompson, R. Paleoclimatic Significance of the Mineral Magnetic Record of the Chinese Loess and Paleosols. *Quat. Res.* **1992**, *37*, 155–170. [CrossRef]
153. Kukla, G.; Heller, F.; Ming, L.X.; Chun, X.T.; Sheng, L.T.; Sheng, A.Z. Pleistocene climates in China dated by magnetic susceptibility. *Geology* **1988**, *16*, 811–814. [CrossRef]
154. Liu, Q.; Deng, C.; Torrent, J.; Zhu, R. Review of recent developments in mineral magnetism of the Chinese loess. *Quat. Sci. Rev.* **2007**, *26*, 368–385. [CrossRef]
155. Heslop, D.; Roberts, A.P. Calculating uncertainties on predictions of palaeoprecipitation from the magnetic properties of soils. *Glob. Planet. Chang.* **2013**, *110*, 379–385. [CrossRef]
156. Maher, B.; Possolo, A. Statistical models for use of palaeosol magnetic properties as proxies of palaeorainfall. *Glob. Planet. Chang.* **2013**, *111*, 280–287. [CrossRef]
157. Polanski, S.; Fallah, B.; Befort, D.J.; Prasad, S.; Cubasch, U. Regional moisture change over India during the past Millennium: A comparison of multi-proxy reconstructions and climate model simulations. *Glob. Planet. Chang.* **2014**, *122*, 176–185. [CrossRef]
158. Jiang, Y.; Xu, Z. On the Spörer minimum. *Astrophy. Space Sci.* **1985**, *118*, 159–162. [CrossRef]
159. Eddy, J.A. The Maunder Minimum. *Science* **1976**, *192*, 1189–1202. [CrossRef] [PubMed]
160. Shindell, D.T.; Schmidt, G.A.; Mann, M.E.; Rind, D.; Waple, A. Solar Forcing of Regional Climate Change During the Maunder Minimum. *Science* **2001**, *294*, 2149–2152. [CrossRef] [PubMed]
161. Huddart, D.; Stott, T. *Earth Environments: Past, Present, and Future*; John Wiley & Sons, Ltd.: West Sussex, UK, 2010; p. 896.
162. Wanner, H.; Beer, J.; Bütikofer, J.; Crowley, T.J.; Cubasch, U.; Flückiger, J.; Goosse, H.; Grosjean, M.; Joos, F.; Kaplan, J.O.; et al. Mid- to Late Holocene climate change: An overview. *Quat. Sci. Rev.* **2008**, *27*, 1791–1828. [CrossRef]
163. Sigl, M.; Winstrup, M.; McConnell, J.R.; Welten, K.C.; Plunkett, G.; Ludlow, F.; Büntgen, U.; Caffee, M.W.; Chellman, N.; Dahl-Jensen, D.; et al. Timing and climate forcing of volcanic eruptions for the past 2500 years. *Nature* **2015**, *523*, 543–549. [CrossRef]
164. Desprat, S.; Goñi, M.F.S.; Loutre, M.-F. Revealing climatic variability of the last three millennia in northwestern Iberia using pollen influx data. *Earth Planet. Sci. Lett.* **2003**, *213*, 63–78. [CrossRef]
165. Bhattacharyya, A.; Sharma, J.; Shah, S.K.; Chaudhary, V. Climatic changes during the last 1800 yrs BP from Paradise Lake, Sela Pass, Arunachal Pradesh, Northeast Himalaya. *Curr. Sci.* **2007**, *93*, 983–987.
166. Miller, G.H.; Geirsdóttir, Á.; Zhong, Y.; Larsen, D.J.; Otto-Bliesner, B.L.; Holland, M.M.; Bailey, D.A.; Refsnider, K.A.; Lehman, S.J.; Southon, J.R.; et al. Abrupt onset of the Little Ice Age triggered by volcanism and sustained by sea-ice/ocean feedbacks. *Geophys. Res. Lett.* **2012**, *39*, L02708. [CrossRef]
167. Xu, H.; Liu, X.; Hou, Z. Temperature variations at Lake Qinghai on decadal scales and the possible relation to solar activities. *J. Atmos. Sol. -Terr. Phys.* **2008**, *70*, 138–144. [CrossRef]
168. Yang, B.; Kang, X.; Bräuning, A.; Liu, J.; Qin, C.; Liu, J. A 622-year regional temperature history of southeast Tibet derived from tree rings. *Holocene* **2010**, *20*, 181–190. [CrossRef]
169. Usoskin, I.G.; Mursula, K.; Kovaltsov, G.A. *Proceedings of the Second Solar Cycle and Space Weather Euroconference, Vico Equense, Italy, 24–29 September 2001*; Sawaya-Lacoste, H., Ed.; ESA SP–477; ESA Publ. Div.: Noordwijk, The Netherlands, 2002; pp. 257–260.
170. Usoskin, I.G.; Solanki, S.K.; Schüssler, M.; Mursula, K.; Alanko, K. Millennium-Scale Sunspot Number Reconstruction: Evidence for an Unusually Active Sun since the 1940s. *Phys. Rev. Lett.* **2003**, *91*, 211101. [CrossRef]
171. Dixit, S.; Bera, S.K. Mid-Holocene vegetation and climatic variability in tropical deciduous sal (Shorea robusta) forest of Lower Brahmaputra valley, Assam. *J. Geol. Soc. India* **2011**, *77*, 419–432. [CrossRef]
172. Dixit, S.; Bera, S.K. Pollen–inferred vegetation vis–à–vis climate dynamics since late Quaternary from Western Assam, Northeast India: Signal of global climatic events. *Quat. Int.* **2013**, *286*, 56–68. [CrossRef]

173. Kaspari, S.; Mayewski, P.; Kang, S.; Sneed, S.; Hou, S.; Hooke, R.; Kreutz, K.; Introne, D.; Handley, M.; Maasch, K.; et al. Reduction in northward incursions of the South Asian monsoon since ∼1400 AD inferred from a Mt. Everest ice core. *Geophys. Res. Lett.* **2007**, *34*, L16701. [CrossRef]
174. He, M.; Yang, B.; Bräuning, A.; Wang, J.; Wang, Z. Tree-ring derived millennial precipitation record for the south-central Tibetan Plateau and its possible driving mechanism. *Holocene* **2013**, *23*, 36–45. [CrossRef]
175. Phadtare, N.R.; Pant, R.K. A century–scale pollen record of vegetation and climate history during the past 3500 years in the Pinder Valley, Kumaon Higher Himalaya, India. *J. Geol. Soc. India* **2006**, *68*, 495–506.
176. Bhattacharyya, A.; Chauhan, M.S. Vegetational and climatic changes during recent past around Tipra bank glacier, Garhwal Himalaya. *Curr. Sci.* **1997**, *72*, 408–412.
177. Kar, R.; Ranhotra, P.S.; Bhattacharyya, A.; Sekar, B. Vegetation vis–à–vis climate and glacial fluctuations of the Gangotri Glacier since the last 2000 years. *Curr. Sci.* **2002**, *82*, 347–351.
178. McDermott, F.; Mattey, D.P.; Hawkesworth, C. Centennial–scale Holocene climate variability revealed by a high–resolution speleothem ð18O record from SW Ireland. *Science* **2001**, *294*, 1328–1331. [CrossRef]
179. Chauhan, M.S.; Mazari, R.K.; Rajagopalan, G. Vegetation and climate in upper Spiti region, Himachal Pradesh during late Holocene. *Curr. Sci.* **2000**, *79*, 373–377.
180. Chauhan, M.S. Late Holocene vegetation and climate change in the alpine belt of Himachal Pradesh. *Curr. Sci.* **2006**, *91*, 1562–1567.
181. Bhattacharyya, A. Vegetation and climate during postglacial period in the vicinity of Rohtang Pass, Great Himalayan Range. *Pollen Et Spores* **1988**, *30*, 417–427.
182. Rawat, S.; Gupta, A.K.; Sangode, S.J.; Srivastava, P.; Nainwal, H.C. Late Pleistocene–Holocene vegetation and Indian summer monsoon record from the Lahaul, Northwest Himalaya, India. *Quat. Sci. Rev.* **2015**, *114*, 167–181. [CrossRef]
183. Chauhan, M.; Sharma, C.; Rajagopalan, G. Vegetation and climate during Late Holocene in Garhwal Himalaya. *J. Palaeosciences* **1997**, *46*, 211–216. [CrossRef]
184. Kotlia, B.S.; Joshi, L.M. Late Holocene climatic changes in Garhwal Himalaya. *Curr. Sci.* **2013**, *104*, 911–919.
185. Yadav, R.R.; Singh, J. Tree-Ring-Based Spring Temperature Patterns over the Past Four Centuries in Western Himalaya. *Quat. Res.* **2002**, *57*, 299–305. [CrossRef]
186. Chaujar, R.K. Climate change and its impact on the Himalayan glaciers—A case study on the Chorabari glacier, Garhwal Himalaya, India. *Curr. Sci.* **2009**, *96*, 703–708.
187. Sanwal, J.; Kotlia, B.S.; Rajendran, C.; Ahmad, S.M.; Rajendran, K.; Sandiford, M. Climatic variability in Central Indian Himalaya during the last ∼1800 years: Evidence from a high resolution speleothem record. *Quat. Int.* **2013**, *304*, 183–192. [CrossRef]
188. Lei, Y.; Tian, L.; Bird, B.W.; Hou, J.; Ding, L.; Oimahmadov, I.; Gadoev, M. A 2540-year record of moisture variations derived from lacustrine sediment (Sasikul Lake) on the Pamir Plateau. *Holocene* **2014**, *24*, 761–770. [CrossRef]
189. Treydte, K.S.; Schleser, G.H.; Helle, G.; Frank, D.C.; Winiger, M.; Haug, G.H.; Esper, J. The twentieth century was the wettest period in northern Pakistan over the past millennium. *Nature* **2006**, *440*, 1179–1182. [CrossRef]
190. Zafar, M.U.; Ahmed, M.; Rao, M.P.; Buckley, B.M.; Khan, N.; Wahab, M.; Palmer, P. Karakorum temperature out of phase with hemispheric trends for the past five centuries. *Clim. Dyn.* **2016**, *46*, 1943–1952. [CrossRef]
191. Chauhan, M.S.; Quamar, M.F. Vegetation and climate change in southeastern Madhya Pradesh during Late Holocene, based on pollen evidence. *J. Geol. Soc. India* **2010**, *76*, 143–150. [CrossRef]
192. Quamar, M.; Chauhan, M. Signals of Medieval Warm Period and Little Ice Age from southwestern Madhya Pradesh (India): A pollen-inferred Late-Holocene vegetation and climate change. *Quat. Int.* **2014**, *325*, 74–82. [CrossRef]
193. Tripathi, S.; Basumatary, S.K.; Singh, V.K.; Bera, S.K.; Nautiyal, C.M.; Thakur, B. Palaeovegetation and climate oscillation of western Odisha, India: A pollen data–based synthesis for the Mid–Late Holocene. *Quat. Int.* **2014**, *325*, 83–92. [CrossRef]
194. Sinha, A.; Cannariato, K.G.; Stott, L.D.; Cheng, H.; Edwards, R.L.; Yadava, M.G.; Ramesh, R.; Singh, I.B. A 900-year (600 to 1500 A.D.) record of the Indian summer monsoon precipitation from the core monsoon zone of India. *Geophys. Res. Lett.* **2007**, *34*, L16707. [CrossRef]
195. Agnihotri, R.; Dutta, K.; Bhushan, R.; Somayajulu, B. Evidence for solar forcing on the Indian monsoon during the last millennium. *Earth Planet. Sci. Lett.* **2002**, *198*, 521–527. [CrossRef]
196. Gupta, A.K.; Das, M.; Anderson, D.M. Solar influence on the Indian summer monsoon during the Holocene. *Geophys. Res. Lett.* **2005**, *32*, LI7703. [CrossRef]
197. Anderson, D.M.; Overpeck, J.T.; Gupta, A.K. Increase in the Asian Southwest Monsoon During the Past Four Centuries. *Science* **2002**, *297*, 596–599. [CrossRef]
198. Chauhan, O.S.; Vogelsang, E.; Basavaiah, N.; Kader, U. Reconstruction of the variability of the southwest monsoon during the past 3 ka, from the continental margin of the southeastern Arabian Sea. *J. Quat. Sci.* **2010**, *25*, 798–807. [CrossRef]
199. von Rad, U.; Schaaf, M.; Michels, K.H.; Schulz, H.; Berger, W.H.; Sirocko, F. A 5000–yr record of climate change in varved sediments from the Oxygen Minimum Zone off Pakistan, northeastern Arabian Sea. *Quat. Res.* **1999**, *51*, 39–53. [CrossRef]
200. Cook, E.R.; Krusic, P.J.; Jones, P.D. Dendroclimatic signals in long tree-ring chronologies from the Himalayas of Nepal. *Int. J. Clim.* **2003**, *23*, 707–732. [CrossRef]
201. Chen, J.; Chen, F.; Feng, S.; Huang, W.; Liu, J.; Zhou, A. Hydroclimatic changes in China and surroundings during the Medieval Climate Anomaly and Little Ice Age: Spatial patterns and possible mechanisms. *Quat. Sci. Rev.* **2015**, *107*, 98–111. [CrossRef]

202. Goosse, H.; Renssen, H.; Timmermann, A.; Bradley, R.S. Internal and forced climate variability during the last millennium: A model-data comparison using ensemble simulations. *Quat. Sci. Rev.* **2005**, *24*, 1345–1360. [CrossRef]
203. Mayewski, P.A.; Maasch, K.A.; Yan, Y.; Kang, S.; Meyerson, E.A.; Sneed, S.B.; Kaspari, S.D.; Dixon, D.A.; Osterberg, E.C.; Morgan, V.I.; et al. Solar forcing of the polar atmosphere. *Ann. Glaciol.* **2005**, *41*, 147–154. [CrossRef]
204. O'Brien, S.R.; Mayewski, P.A.; Meeker, L.D.; Meese, D.A.; Twickler, M.S.; Whitlow, S.I. Complexity of Holocene Climate as Reconstructed from a Greenland Ice Core. *Science* **1995**, *270*, 1962–1964. [CrossRef]
205. Yang, B.; Qin, C.; Wang, J.; He, M.; Melvin, T.M.; Osborn, T.J.; Briffa, K.R. A 3,500-year tree-ring record of annual precipitation on the northeastern Tibetan Plateau. *Proc. Natl. Acad. Sci. USA* **2014**, *111*, 2903–2908. [CrossRef] [PubMed]
206. Tan, L.; Cai, Y.; An, Z.; Yi, L.; Zhang, H.; Qin, S. Climate patterns in north central China during the last 1800 yr and their possible driving force. *Clim. Past* **2011**, *7*, 685–692. [CrossRef]
207. Cook, E.R.; Anchukaitis, K.J.; Buckley, B.M.; D'arrigo, R.D.; Jacoby, G.C.; Wright, W.E. Asian Monsoon Failure and Megadrought During the Last Millennium. *Science* **2010**, *328*, 486–489. [CrossRef] [PubMed]
208. Thompson, L.G.; Yao, T.; Mosley-Thompson, E.; Davis, M.E.; Henderson, K.A.; Lin, P.-N. A high–resolution millennial record of the South Asian Monsoon from Himalayan ice cores. *Science* **2000**, *289*, 1916–1919. [CrossRef] [PubMed]
209. Thompson, L.G.; Mosley-Thompson, E.; Davis, M.E.; Lin, P.-N.; Henderson, K.; Mashiotta, T.A. Tropical glacier and ice core evidence of climate change on annual to millennial time scales. *Clim. Chang.* **2003**, *59*, 137–155. [CrossRef]
210. Thompson, L.G.; Yao, T.; Davis, M.E.; Henderson, K.A.; Mosley-Thompson, E.; Lin, P.-N.; Beer, J.; Synal, H.-A.; Cole-Dai, J.; Bolzan, J.F. Tropical Climate Instability: The Last Glacial Cycle from a Qinghai-Tibetan Ice Core. *Science* **1997**, *276*, 1821–1825. [CrossRef]
211. Thompson, L.G.; Mosley-Thompson, E.; Brecher, H.; Davis, M.; León, B.; Les, D.; Lin, P.-N.; Mashiotta, T.; Mountain, K. Abrupt tropical climate change: Past and present. *Proc. Natl. Acad. Sci. USA* **2006**, *103*, 10536–10543. [CrossRef] [PubMed]
212. Thompson, L.G.; Yao, T.; Davis, M.E.; Mosley-Thompson, E.; Mashiotta, T.A.; Lin, P.N.; Mikhalenko, V.N.; Zagorodnov, V.S. Holocene climate variability archived in the Puruogangri ice cap on the central Tibetan Plateau. *Ann. Glaciol.* **2006**, *43*, 61–69. [CrossRef]
213. Pages 2k Consortium. Continental–scale temperature variability during the past two millennia. *Nat. Geosci.* **2013**, *6*, 339–346. [CrossRef]
214. Tan, M.; Liu, T.; Hou, J.; Qin, X.; Zhang, H.; Li, T. Cyclic rapid warming on centennial-scale revealed by a 2650-year stalagmite record of warm season temperature. *Geophys. Res. Lett.* **2003**, *30*, 1617. [CrossRef]
215. Ge, Q.; Hao, Z.; Zheng, J.; Shao, X. Temperature changes over the past 2000 yr in China and comparison with the Northern Hemisphere. *Clim. Past* **2013**, *9*, 1153–1160. [CrossRef]
216. McKay, N.P.; Kaufman, D.S. An extended Arctic proxy temperature database for the past 2,000 years. *Sci. Data* **2014**, *1*, 140026. [CrossRef]
217. Christiansen, B.; Ljungqvist, F.C. The extra-tropical Northern Hemisphere temperature in the last two millennia: Reconstructions of low-frequency variability. *Clim. Past* **2012**, *8*, 765–786. [CrossRef]
218. Crowley, T.J. Causes of Climate Change Over the Past 1000 Years. *Science* **2000**, *289*, 270–277. [CrossRef]
219. Esper, J.; Cook, E.R.; Schweingruber, F.H. Low-Frequency Signals in Long Tree-Ring Chronologies for Reconstructing Past Temperature Variability. *Science* **2002**, *295*, 2250–2253. [CrossRef]
220. D'Arrigo, R.; Wilson, R.; Jacoby, G. On the long-term context for late twentieth century warming. *J. Geophys. Res. Atmos.* **2006**, *111*, D3. [CrossRef]
221. Ammann, C.M.; Wahl, E.R. The importance of the geophysical context in statistical evaluations of climate reconstruction procedures. *Clim. Chang.* **2007**, *85*, 71–88. [CrossRef]
222. Moberg, A.; Sonechkin, D.M.; Holmgren, K.; Datsenko, N.M.; Karlén, W. Highly variable Northern Hemisphere temperatures reconstructed from low- and high-resolution proxy data. *Nature* **2005**, *433*, 613–617. [CrossRef] [PubMed]
223. Mann, M.E.; Zhang, Z.; Hughes, M.K.; Bradley, R.S.; Miller, S.K.; Rutherford, S.; Ni, F. Proxy-based reconstructions of hemispheric and global surface temperature variations over the past two millennia. *Proc. Natl. Acad. Sci. USA* **2008**, *105*, 13252–13257. [CrossRef] [PubMed]
224. Mann, M.E.; Jones, P.D. Global surface temperatures over the past two millennia. *Geophys. Res. Lett.* **2003**, *30*, 1820. [CrossRef]
225. Pradhan, K.C.; Sharma, E.; Pradhan, G.; Chettri, A.B. *Sikkim Study Series: Geography and Environment*; Information and Public Relations Department, Government of Sikkim: Sikkim, India, 2004; Volume 1, p. 366.
226. Owen, L.A.; Benn, D.I.; Derbyshire, E.; Evans, D.J.A.; Mitchell, W.A.; Richardson, S. The Quaternary glacial history of the Lahul Himalaya, Northern India. *J. Quat. Sci.* **1996**, *11*, 25–42. [CrossRef]
227. Wien, K. *Zur Karte des Zema–Gletschers*; Zschr. f. Glkde, Bd. XXI; Leipzig, Germany, 1934. (In German)
228. Thorarinsson, S. Present Glacier Shrinkage, and Eustatic Changes of Sea–Level. *Sigurdur Geogr. Ann.* **1940**, *22*, 131–159.

Supplementary Information

Revisit the Medieval Warm Period and Little Ice Age in proxy records from Zemu glacier sediments, Eastern Himalaya: vegetation and climate reconstruction

Nivedita Mehrotra [1], Nathani Basavaiah [2] and Santosh K. Shah [1,*]

[1] Birbal Sahni Institute of Palaeosciences, 53 University Road, Lucknow – 226007, India;
[2] Indian Institute of Geomagnetism, Navi Mumbai, Maharashtra, India;
* Correspondence: santoshkumar_shah@bsip.res.in; santoshk.shah@gmail.com

Materials and Methods

Surface and Sub–surface sediment sampling

To study modern pollen distribution in the region, 20 moss cushion samples were collected from the Lachen to Zemu transect and adjoining areas (Figure 1). The sites were selected from lower to higher elevations, ranging from 2600 to 4311 m. The locations of these sites ranged from the temperate forest belt to the alpine and above the tree line, close to the glacier. The details of the moss cushion sample sites, along with dominant forest types and climate, are given in Table S1.

A sub-surface sediment profile of 127 cm depth was collected after digging a pit at Yabuk (27°45′52.1″ N latitude and 88°23′47.7″ E longitude) at an elevation of 4016 m. This site is approximately 1.2 km down the valley from the snout of the Zemu glacier. This site is within the Khangchendzonga National Park (Biosphere Reserve), established in the year 1977 and considered to be one of the most significant protected areas in the entire Himalayan region. The location of the fossil sites considered here is shown in Figure 1. In total, 41 samples were collected at various intervals depending on the nature of the sediments in the profile. Lithologically, this profile is characterized by upper 0–40 cm coarse sand mixed with fine sand and silty clay with some gravel pieces. From about 40–64 cm, the sediments were made up of clay rich in organic matter, silty clay, and black clay intermixed with some gravel pieces. Coarse sand, gravel, and silty clay start to occur from 64 cm and are found until 107 cm, from where they begin to be coarser and occur along with silty clay further up to 113 cm. Fine sand along with silty clay then continues from 113 to 127 cm, i.e., up to the bottom end of the profile. A palynological analysis was carried out on 21 samples where finer grained sediments are prominent in this mostly sand-dominated sediment profile. Coarser sediment layers were considered for other analyses.

Pollen analysis

The samples for pollen analysis for both modern and fossil samples were processed using the standard procedure of palynological analysis with HCl, KOH, HF, and Erdtman's acetolysis [114]. A minimum of 300 pollen grains per sample were counted and pollen sum and total pollen counts were calculated based on the pollen/spore grain counts. The percentages of tree, shrub, and herb taxa were calculated using pollen sum, excluding ferns and aquatic taxa. The total pollen count was calculated using counts of all the pollen/spores, which include arboreal and non-arboreal taxa, aquatic, and fern

Table S1. Sampling site details of the modern pollen data along with climatic variables and dominant forest and vegetation types

SC	LAT	LONG	ELEV	LN	MAT	MTCO	MTWA	MAP	Dominant forest type/vegetation
SKM022	27° 45' 44.6"	88° 33' 06.9"	2600	Zema I	10.57	2.58	16.35	145.48	*Abies densa-Tsuga dumosa-Hippophae*
SKM031	27° 44' 19.6"	88° 32' 51.2"	2741	Between Lachen and Zema I	9.82	1.77	15.74	138.93	*Picea spinulosa-Hippophae*
SKM034	27° 43' 35.5"	88° 32' 48.9"	2814	Above Chaten	9.42	1.34	15.40	136.71	*Picea spinulosa-Abies densa-Rhododendron spp*
SKM039	27° 45' 55.4"	88° 31' 26.8"	2843	Zema II	9.23	1.15	15.21	138.43	*Abies densa-Tsuga dumosa-Hippophae*
SKM046	27° 46' 28.1"	88° 30' 39.6"	3057	Between Zema II and Dozom Khola	8.08	-0.10	14.29	128.64	*Abies densa*
SKM049	27° 46' 50.3"	88° 30' 12.1"	3166	Dozom Khola	7.50	-0.73	13.82	123.52	*Abies densa*
SKM054	27° 46' 57.9"	88° 29' 19.3"	3303	Talem	6.77	-1.53	13.24	116.52	*Abies densa-Juniperus indica*
SKM058	27° 46' 48.1"	88° 28' 20.3"	3501	1 km after Talem	5.72	-2.68	12.42	105.01	*Abies densa-Juniperus indica*
SKM060	27° 46' 40.9"	88° 27' 54.0"	3510	1 km before Jakthang	5.67	-2.74	12.39	103.77	*Abies densa-Juniperus indica*
SKM065	27° 46' 22.6"	88° 27' 00.4"	3504	Jakthang	5.70	-2.72	12.45	101.47	*Abies densa-Juniperus indica*
SKM069	27° 46' 08.9"	88° 26' 01.1"	3621	1 km after Jakthang	5.06	-3.30	11.75	109.72	*Abies densa-Juniperus indica*
SKM074	27° 45' 47.5"	88° 24' 40.7"	3793	Between Jakthang and Yabuk	4.15	-4.28	11.01	101.91	*Abies densa-Juniperus indica*
SKM077	27° 45' 49.7"	88° 24' 06.0"	3915	1 km before Yabuk	3.51	-4.99	10.49	95.91	*Abies densa-Juniperus indica-Rhododendron*
SKM081	27° 46' 06.8"	88° 22' 50.2"	4253	Zemu glacier	1.75	-7.02	9.30	62.56	*Juniperus squamata*
SKM087	27° 46' 06.0"	88° 23' 09.2"	4132	Yabuk	2.39	-6.34	9.84	66.68	*Abies densa-Rhododendron*
SKM090	27° 45' 59.1"	88° 23' 21.9"	4050	Yabuk	2.82	-5.87	10.18	71.03	*Abies densa-Rhododendron*
SKM101	27° 46' 07.1"	88° 22' 33.9"	4311	Sona Camp	1.44	-7.35	9.03	60.94	*Juniperus squamata*
SKM105	27° 54' 27.0"	88° 31' 28.8"	4016	Chopta valley	3.02	-5.71	10.27	79.04	*Betula utilis-Juniperus-Rhododendron*
SKM108	27° 52' 20.8"	88° 32' 35.2"	4019	Thangu	3.01	-5.76	10.29	76.32	*Betula utilis-Juniperus-Rhododendron-Abies densa*
SKM116	27° 50' 40.2"	88° 33' 00.2"	3608	Yathang	5.17	-3.33	11.97	99.92	*Betula utilis-Juniperus-Rhododendron-Abies densa*

SC = Sample code; LAT = Latitude °N; LONG = Longitude = °E; ELEV = Elevation in meter; LN = Locality name; MAT = mean annual temperature (°C); MTCO = mean temperature of coldest month (°C); MTWA = mean temperature of warmest month (°C); MAP = mean annual precipitation (mm)

spores. Pollen spectra for modern pollen samples and pollen percentage diagrams for fossil samples were prepared using computer software, TILIA version 2.0.2 [115]. For the fossil pollen, the pollen diagram was divided into pollen assemblage zones (YAB) along with subzones, if necessary, based on the stratigraphically constrained cluster analysis [116] CONISS in the TILIA computer program. The pollen taxa with more than 0.5% were included in the CONISS analysis to prepare zonation, to maintain standardization and consistency in the data, and reduce bias. The CONISS analysis applies stratigraphically constrained chord-distance clustering to square-root-transformed pollen percentage data. However, for modern pollen datasets, unconstrained chord distance clustering on square-root-transformed pollen percentage data was applied to group the modern sampling sites.

Mineral magnetism analysis

Sediments were prepared for magnetic measurements by oven drying at a temperature no more than 40°C overnight, as a higher temperature may cause changes in the magnetic mineralogy. Dry samples were then crushed and disaggregated gently by using a pestle, wrapped in a clean cling foil, and packed tightly into standard 10 cc cylindrical plastic holders. For the mass specific magnetic parameters, the mass of the sample was calculated by taking the weight difference between empty bottles along with thin cling foil and bottles packed with sample material.

All mineral magnetic measurements were made on the entire profile constituting 41 samples at the environmental magnetism laboratory, Indian Institute of Geomagnetism, Navi Mumbai, following the methodology and procedure given in Basavaiah [91] and Basavaiah and Khadkiar [90]. Low and high-frequency magnetic susceptibility (χLF at 0.976 kHz and χHF at 1.6 kHz with units of 10^{-8} m^3/kg) measurements were made using AGICO MFK1 Kappabridge to indicate the concentration and type of magnetic minerals in the sample. Frequency-dependent susceptibility, expressed as a percentage of χLF% (FD%), was calculated to indicate the concentration of ultra-fine-grained ferrimagnetic magnetic minerals (grain size approx. 0.02 um). Anhysteretic and isothermal remanent magnetizations (ARM and IRM) were measured on the Molspin spinner magnetometer. ARM was imparted in a DC bias field of 0.1 mT with a peak AF field of 100 mT. Susceptibility of ARM (χARM, 10^{-5} m^3/kg) was calculated by dividing the ARM by the DC bias field. Saturation IRM (SIRM, 10^{-5} Am^2/kg) was induced using a Molspin pulse magnetizer. Ratio measurements of S–Ratio ($IRM_{-0.3}$/SIRM), Soft IRM (SIRM-IRM_{-20}), and Hard IRM (SIRM-$IRM_{-0.3}$) give an indication of the type of magnetic minerals (i.e., ferrimagnetic or canted–antiferromagnetic). The inter-parametric ratios (SIRM/ARM and SIRM/χLF) were used to infer the relative variations in magnetic grain size. The ratio ARM/SIRM increases as magnetic grain size decreases, and is particularly sensitive to SD and small PSD grain sizes. Most hematite, which is weakly magnetic compared to magnetite, occurs as SD grains [89,91] that yield high ratios of ARM/SIRM.

Chronology and age–depth model

Two sub-surface sediment samples at depths of 57–60 cm and 45–47 cm have been dated as 1030±80 yrs BP and 540±80 yr BP, respectively, at the radiocarbon Laboratory of the Physical Research Laboratory, Ahmedabad, India. Sediment at the bottom part of the profile could not be dated due to insufficient carbon for ^{14}C dating. These two dates suggest that the profile is of Late Holocene age. The ^{14}C dates were calibrated using Oxcal version 4.2 [117]. Using these two dates in two different depths, both ^{14}C dates and calibrated age in cal years BP and BC/AD were interpolated and extrapolated for each sample of the fossil sediment profile. Details of the chronology of the sediment profile are

provided in Table 2.

Modern climate

To establish modern pollen–climate relationships and subsequently develop transfer function models, climatic data (temperature and precipitation) from meteorological stations is a pre-requisite. These climate data are required to estimate the monthly and bioclimatic variables of modern pollen sites. For this, we screened the climate records of the study site and adjoining regions based on their length, homogeneity, and completeness of data. The climatic data were available from the India Meteorological Department (IMD), Pune and Global Historical Climate Network version 2 (GHCN v2), and hydropower reports of the National Hydroelectric Power Corporation (NHPC). We observed that the number of meteorological stations with both temperature and precipitation records was small and mostly located at lower elevations. Apart from two meteorological stations, Gangtok and Tadong, where fully-fledged meteorological observatories have been functioning since 1957 and 1978, respectively, other stations were mainly rain gauge stations and records are available for approximately 4 to 25 years [111] (Figure 2). The records from the higher elevation station have a maximum number of missing data and discontinuities in the observation. Among these, only one station, Gangtok (Figure 1 and 2), had climate data available for more than 30 years with few missing values [118], but is located at a lower elevation and is very far from the present study region.

The climate for each modern pollen site is best interpolated using a large number of homogenous climate stations, which is not possible here due to the lack of sufficient meteorological stations in the entire Sikkim Himalayan region. Thus, we used global land areas and a high-resolution climate data set by New et al. [119] to estimate modern pollen site-specific climate. The dataset by New et al. [119] has a resolution of (10 arc–minutes/~18 km/~0.17°) and is based on the Climate Research Unit (CRU) gridded climate dataset, with spatial interpolation used for regions with no data. Temperature and precipitation records were extracted for 42 grid points covering the entire Sikkim region and adjoining areas (Figure 2). We compiled various climatic variables such as mean annual temperature (MAT), mean temperature of the coldest month (MTCO), mean temperature of the warmest month (MTWA), and mean annual precipitation (MAP) based on gridded temperature and precipitation records. We selected these priori climatic variables to develop the transfer function, as these climatic variables are widely used in proxy climate calibration, palaeoclimatic reconstructions, and climate modeling [53]. The range of distribution of these climatic variables over Sikkim and adjoining regions is shown in Figure 3. The elevation gradient of these climate grid points ranges from 875 m to 6486 m. The minimum and maximum values for climatic variables are (MAT, –10.3 to 19.5°C; MTCO, –19.4 to 12.2°C; MTWA, –1.5 to 23.6°C and MAP, 215.7 to 3341.7 mm). The modern pollen site-specific values for MAT, MTCO, MTWA, and MAP were interpolated using a weighted distance interpolation procedure after reducing all stations to sea level [120]. This technique takes into account all climate stations (here, 10–minute latitude/longitude grids points) within the interpolation radius of the pollen sampling sites. The weighted distance interpolation technique yields estimates of temperature variables (MAT, MTCO, and MTWA) with r^2 of > 0.996 and precipitation variables (MAP) with r^2 = 0.955.

Numerical analysis and palaeoclimatic reconstruction

Numerous transfer functions have been developed for quantitative reconstruction of palaeoenvironmental variables using varieties of proxies [38,70,72,73,76,77,121]. However, before performing quantitative climate reconstruction, the relationship between biological assemblages along the climatic gradient of interest need to be assessed to determine whether they follow linear-based or unimodal-based statistical methods [38] using the ordination technique. This was accomplished by estimations using the detrended correspondence analysis (DCA). The gradient lengths were determined in DCA on the complete percentage-square-root-transformed pollen dataset. The pollen percentage data were square–root-transformed to stabilize the variance and to minimize the 'signal-to-noise' ratio in the data [44,122]. The estimated gradient length of the environmental variables expressed in standard deviation units is an estimate of the behavior of the pollen taxa along the length of this gradient. Based on this gradient length, the appropriate ordination model to explore the relationship between modern pollen taxa and various climatic variables was selected. If the gradient length is > 2.5 standard deviation, unimodel responses are suitable [38] and canonical correspondence analysis (CCA) should be used. In case of gradient length < 2.5, linear-based methods such as the principal component analysis (PCA) and redundancy analysis (RDA) are appropriate. In this linear ordination approach, PCA is used to understand the underlying data structure, and unconstrained analysis and RDA are used along with the climatic variable to check its quantitative influence on the datasets. The RDA distinguishes the amount of variation in the pollen datasets, explained by climatic datasets as a constrained form of ordination analysis. The Monte Carlo permutation tests (using 999 random permutations) were used to determine statistical significance in the ordination. All ordination analyses were carried out in program CANOCO, version 5 [123].

In the ordination analysis, to eliminate the effect of high co-linearity among the environmental variables, variance inflation factors (VIFs) were calculated for each environmental variable. If the VIF value of a variable is higher than 20, this indicates that the variable is co-linear with the other variables and captures little variance [124,125]. After screening the climatic variables MAT, MTCO, MTWA and MAP for VIF values, we observed co-linearity among them. The analysis was then repeated, and screening for the VIF value was carried out each time after removing environmental variables based on the lowest correlation with axis 1 and until all VIF values were lower than 20. After repeating the analysis, values for MAP and MTWA were found to be lower than 20. Thus, these two climatic variables are considered to have a significant relationship with the pollen data and have a unique influence on the distribution of pollen assemblages in the studied region. Furthermore, to identify the dominant controls of the environment on pollen datasets in the study area, climatic variables MAP and MTWA were selected. The observed relationships were then applied for quantitative climate reconstructions using the fossil pollen assemblage in sub-surface sediments through the pollen–climate transfer function.

The transfer function model was carried out using an established numerical method commonly used in palaeoecology and palaeoclimatic studies. However, care has been taken to select the transfer function model based on the linear or unimodel response observed between pollen taxa and climate variables. In the DCA, the gradient length was found to be consistently short (<1.5 standard deviation), suggesting that the response curves are linear or at least monotonic [126]; thus, linear methods are more appropriate and were selected for the present study [38]. Therefore, the method of partial least square regression (PLS) [37,127] was used to develop the pollen–climate transfer function for MTWA and for its quantitative reconstruction during the Late Holocene.

The PLS method is considered a linear method [37,38,127]. It helps to remove the co-linearity that persisted among the predictor variable (pollen taxon) by using orthogonal components. The orthogonal components are obtained from the singular decomposition of the response variable (climate) and predictor variable (pollen taxon). In this method, the response variable is used in the initial component decomposition, which improves the similar principal components [128]. The PLS approach calculates the transfer function by inverse regression, which relates the modern pollen datasets to the climate variables. This function can then be applied to predict climatic variables from fossil assemblages.

The PLS model was verified using the leave-one-out cross-validation procedure [37,129], using the first x (x=1–6) components to determine the optimum transfer function and to detect the samples with large residuals. In the leave-one-out cross-validation procedure, each pollen sample was systematically removed from the training set and the observed climate was predicted using the remaining pollen samples (n–1). The PLS model's performance was assessed in terms of statistical criteria such as the root mean square error for prediction (RMSEP) and the coefficient of determination (r^2) of observed versus predicted values. The RMSEP indicates the systematic differences in predicted error, whereas the r^2 measures the strength of the relationship between observed and predicted values. The number of PLS components included was selected on the basis of the lowest RMSEP and highest r^2 between observed and predicted values [37,38,67]. Prior to final PLS model development, samples were scrutinized for outlier values (large residuals), which were removed from the final transfer function. In both the original and final screened datasets, RMSEP and r^2 were calculated. The sample-specific error for reconstruction was conducted by applying 1000 bootstrap cycles. The quantitative climate reconstructions are carried out using the transfer functions model developed in R version 3.2.0 [130] using the *rioja* package [131].

Results

Modern pollen sites and assemblages

Based on the modern surface samples (SKM), we recovered 34 pollen taxa, comprising both arboreal and non-arboreal, and 27 taxa were present with >0.5 % in at least two samples. The distributions of the abundant taxa are presented as modern pollen spectra (Fig. 4). Based on the CONISS on the percentage of modern pollen data, two cluster groups were identified and their vegetation composition was represented accordingly.

Fossil pollen assemblage

Pollen zone YAB–I (126–99.5 cm, 2992–2188 cal years BP, BC 1042–238): This zone was at the depth 126–99.5 cm and included the samples obtained in Yabuk: 41, 39 and 29, with an age range of 2992–2188 cal years BP (BC 1042–238). Due to the presence of excessive sand and no yield of pollen grains, many of the samples in this zone were not analyzed for pollen spectra. This zone was dominated by tree elements such as Magnoliaceae (78%–40%), Juniper (29–16%), and *Larix* (21–19%). Other tree taxa such as Juglandaceae, *Quercus* (3.5–0.23%) were also included in the pollen spectra. The lower part of this zone has less than 1% of *Abies* (0.20%), *Pinus* (0.86%), *Alnus* (0.20%), and *Salix* (0.38%), marking the presence of these taxa. The herbaceous and shrub taxa present in this zone are sparse species such as Asteraceae–Tubuliflorae (1.5%–0.70%), Apiaceae (0.19%–0.13%), Caryophyllaceae (0.38–0.07%) and

Euphorbiaceae (0.19%) and are present along with about 0.10–0.03% of Tiliaceae, Asteraceae–Liguliflorae, and *Artemisia*, Lamiaceae. Aquatic taxa evident in this zone were *Impatience* (1.06–0.68%). Fern spores such as Monolete (57–6.38%) and Trilete (0.74–0.05%) were highest in comparison to the consecutive zones above.

Pollen zone YAB–II (78.5–41.5 cm, 1551–509 cal years BP, AD 399–1441): The zone YAB II from a depth in the range 94.5–41.5 cm is of 1551–509 cal years BP (AD 399–1441). This zone was further subdivided into YAB II (a) and YAB II (b). These are further described below.

Pollen zone YAB–II (a): This sub zone was from about 78.5 to 61cm, with an age range of 1551 cal years BP (AD 399) up to 1121 cal years BP (AD 929). In this zone, again, there is a clear dominance of certain tree taxa such as *Larix* (67.50–9.15%), *Corylus* (60–5.45%), Juniper (6.57–2.08%), *Betula* (4.87–0.51%), and *Quercus* (2.29–1.70%). The broad-leaved taxa Magnoliaceae (3.34–1.74%) was comparatively less evident, whereas Rhododendron (10.72– 1.35%), *Salix* (1.84–0.08%), *Alnus* (5.66–2.09%), and *Tsuga* (2.59–2.16%) increased, as seen in zone YAB–I below. *Pinus* (1.32–0.93%), *Abies* (0.97–0.29%), and *Picea* (0.12–0.05%) conifer taxa were more dominant than in the previous zone YAB–I. The dense forest cover had ground covered with herbs such as Asteraceae–Tubuliflorae (2.09–0.89%), less than 0.5% of *Artemisia*, Caryophylaceae, Apiaceae, *Epilobium*, Euphorbiaceae, Lamiaceae and shrubs of *Viburnum*, Oleaceae, and Solanaceae. The small-sized (< 50μ) Poaceae (0.02%) was only found in the upper parts of this zone. Aquatic taxa *Impatience* (0.22–0.08%) and *Potamogeton*(0.02%) were relatively lower than zone YAB–I below, as were spores such as Monolete (2.58–0.80%) and Trilete (0.07–0.22%), which became more evident from this zone onwards.

Pollen zone YAB–II (b): This zone was marked at a depth of 56–41.5 cm with an age range from 869 Cal years BP (AD 1081) to 509 cal years BP (AD 1441) and a mixed plant element. The trees dominant in this zone are *Larix* (27.41–12.46%), *Corylus* (25.16–3.10%), and Magnoliaceae (31.91–9.62%), more than in the zone below. Rhododendron was at its maximum in this zone compared to all other zones (15.28–2.45%). Juniper (11.02–5.37%), *Salix* (12.95–1.05%), *Alnus* (5.48–4.89%), and *Tsuga* (8.52–2.88%), were found more than in zone YAB–II (a) below. *Pinus* (4.97–1.44%), *Abies* (3.35–0.42%), *Betula* (3.9–0.68%), *Quercus* (4.69–1.69%), Juglandaceae (2.19–0.08%), and *Acer* (1.14–0.06%) were the other tree taxa evident. The aquatic taxa *Impatience* (2.45– 0.14%) and ferns, i.e., Monolete (26.27–9.40%) and Trilete (2.31–0.22%), were also present. Less than 0.5% of *Viburnum*, Oleaceae, Asteraceae–Liguliflorae, Lamiaceae, Primulaceae, Cyperaceae, and Poaceae (<50μ) were found, along with about 3–1% of Apiaceae, *Galium*, *Artemisia*, Caryophylaceae, and Asteraceae–Tubuliflorae (5–1%).

Pollen zone YAB–III (38.5–1 cm, 472–0 cal years BP, AD 1478–1950): This zone had the most recent sediments at depths of 38.5 cm at the bottom and 1cm at the top, with an age range of 472 cal years BP to the present (AD 1950). This zone was further divided into YAB III (a) and YAB III (b) at depths of 38.5–29.5 cm and 24.5–1cm, respectively. This zone showed the presence of dense forest near or in close proximity to the valley, with extensive tree elements, and the ground was covered in herbaceous taxa. The details of the zone are given below.

Pollen zone YAB–III (a): This zone is aged about 472–358 cal years BP (AD 1478–1592) and has fewer trees and more ground elements, especially herbs. The tree taxa are evident more than any other zone, mainly dominated by Magnoliaceae (45.28–13.10%), *Larix* (29.47–19.97%), Juniper (17.37–9.43%),

Tsuga (7.55–0.32%), and *Quercus* (7.51–1.23%). Other taxa such as *Alnus*, *Salix*, *Betula*, Juglandaceae, and *Rhododendron* ranged from 3 to 1%, while *Corylus* and other conifers such as *Abies*, *Picea*, and *Pinus* were less than 1%. Herbs constitute approximately 32–7.55% of this zone and are dominated by Apiaceae (29.55–1.89%), Asteraceae–Tubuliflorae (2.25–0.88%), *Artemisia* (1.03–0.16%), and Caryophyllaceae (2.11–016%), and about less than 1% of *Primula*, *Epilobium*, Lamiaceae, Euphorbiaceae, Asteraceae–Liguliflorae. Solanaceae (1.60%), and *Viburnum* (0.16%) comprised the shrub taxa found here. The grass pollen, i.e., Poaceae <50μ (3.68–0.37%), was evident, but Cyperaceae (3.77%) and larger grasses, i.e., Poaceae >50μ (0.33%), marked their presence. Aquatic taxa such as *Impatience* (5.75–1.37%) and *Potamageton* (0.85–0.39%) were highest (6–1%) in the latter part of the zone compared to the underlying and subsequent zones. Monolete Fern (26.03–11.76%) was also present in high amounts in this zone.

Pollen zone Yabuk III (b): This zone has an age range of and is completely dominated by tree taxa. The trees were mostly Juniper (42.71–8.6%), *Larix* (45.55–22.66%), Magnoliaceae (29.68–17.18%), *Corylus* (11.83–1.05%), *Betula* (5.26–0.26%), *Alnus* (5.16–2.90%) and Fabaceae (4.76–0.53%). About 3–1% of *Pinus*, *Tsuga*, Juglandaceae, *Rhododendron*, *Salix*, and *Abies*, and less than 1% of *Abies*, *Picea*, and *Quercus* comprise the rest of the trees found in this zone. Very few shrubs, specifically *Viburnum* (2.041%), Oleaceae (2–0.68%), and Solanaceae (0.21%), were present. Few herbaceous elements in contents of 3–1%, namely Caryophyllaceae (3–1%), Apiaceae (2%), Asteraceae–Tubuliflorae (2–1%), Primulaceae (1.05%), Euphorbiaceae (1%), and less than 1% of *Galium*, *Artemisia*, Asteraceae–Liguliflorae, and *Epilobium,* were found. Grass pollen such as Poaceae <50μ (6–0.26%) and Cyperaceae (0.53%) occurred along with cultivated elements, i.e., Poaceae >50μ (1%) were present in this zone. Aquatic taxa, which were consistently as high as in the previous zones, included *Impatience* (4.24–0.19%) and *Potamageton* (5–0.46%). Ferns were lesser than in the previous zone, i.e., Monolete (16.42–5.81%) and Trilete (1–0.22%).

Magnetic parameters, fossil pollen-zones and quantitative palaeoclimate

Pollen zone YAB–I (126–99.5 cm, 2992–2188 cal years BP, BC 1042–238): This zone is characterized by decreasing χLF, XARM, SIRM, and S–ratio values, indicating decreasing proportions of low-coercivity magnetic minerals (magnetite) with increasing amounts of high-coercivity minerals (hematite) in the topmost part of the zone. FD% showed low values first and later demonstrated increasing values from the middle interval (115–90 cm), indicating high amounts of weathered minerals in the top part of the zone. The ARM/SIRM ratio decreased from the base to the top of the zone, indicating high proportions of large MD (magnetite) and detrital high-coercivity minerals, as reflected in the S-Ratio. Concurrent trends were also observed in the pollen analysis. More pollen taxa were observed in samples with higher ferrimagnetic content intervals (130–115 cm). These inferences are also similar to the MAP and MTWA reconstructions, where the higher precipitation and temperature coincide with increased detrital hematite content and vice versa with magnetite (Figure 9).

Pollen zone YAB–II (78.5–41.5 cm, 1551–509 cal years BP, AD 399–1441): In this zone, the χLF values are generally low, with a slight decreasing trend at the top of the zone. The FD% are variable, with an overall decreasing trend at the top of the zone, but extremely high values can be seen at ~44 cm depth (509 cal years BP, AD 1441). The SIRM values are low initially and then moderate towards the end of this zone. At the interval (65 – 40 cm), a high SIRM/χLF ratio, hard IRM, and low S-Ratio indicate increasing proportions of hematite in the sediments in the middle part of the zone. Similar observations

were made for the XARM and ARM/SIRM ratios, which oscillate from low to high, before lowering further, indicating the increased contribution of fine-grained ferrimagnetic minerals in the interval (65–55 cm), followed by high proportions of larger MD high-coercivity minerals (hematite). This might be due to the increased precipitation and higher temperature in the region. The S-ratio also coincides with the variation in the MAP reconstruction, and the initially high S-ratio fluctuates, decreases, and later rises (Figure 9), indicating water saturation of the soil and a changing redox state, thereby forming magnetite of possible microbial origin during periods of enhanced precipitation. Here, we must also consider the fact that snow melt and/or glacial melt waters also help to retain the soil's moisture content at a high level in times of low precipitation and high temperatures. This might also contribute to the high S-ratio values.

Pollen zone YAB–III (38.5–1 cm, 472–0 cal years BP, AD 1478–1950): This zone begins with low χLF and high FD%, later fluctuating throughout the zone. The overall magnetic mineral content is high in this zone compared to the underlying zone. During the beginning of this zone or the termination of MWP, low values of χARM and SIRM, along with χLF, signify the low concentration of ferrimagnetic minerals as the warmer phase ends. The ARM/SIRM ratio as this zone starts, and oscillating SIRM, Soft IRM, and S–ratio from high to low, and high values indicate the presence of predominantly fine-grained ferrimagnetic minerals (magnetite). However, as the LIA begins, during which χLF, FD%, XARM, and SIRM increase, then decrease and further rise towards the recent sediments. This extensive fluctuation is due to prevailing cold, dry conditions changing to higher snowfall (precipitation), which later reduces. Therefore, the magnetite (MD grain) constituent that is dominant in this period has low ARM/SIRM ratios and HIRM values, along with higher S-ratios. In this zone, the precipitation fluctuates along with the lowering temperature in the reconstruction of MAP and MTWA, which is captured clearly in the χLF and SIRM values (Figure 9).

Discussion

Climate reconstructions comparison – qualitative approach

The climatic variability during the MWP and LIA time periods, recorded in the present pollen-based climate reconstructions, is comparable with other pollen and proxy-based studies carried out in different regions of India, the Himalayas, and the adjoining oceanic region. The time span and climatic inference made for the MWP and LIA periods in these studies are presented in Figure 10 and Figure 11, respectively, and are described in the following section.

There are only a few pollen-based records available in the eastern Himalayas for the Late Holocene [25]. The pollen record from Kupup Lake, eastern Sikkim [85], recorded a cold-dry climate during the years 1800–1450 BP (BC 150–AD 500). The climate of Kupup became warm and moist during 1450–450 cal years BP (AD 500–1500) and reverted to colder and drier conditions during 450–200 cal years BP (AD 1550–1750); which corresponds to the climate oscillation signals of MWP and LIA, respectively. Furthermore, the climate became cold and moist until recently. The recent cold and moist climate observed in Kupup Lake is similar to the present climate reconstructions. Another pollen record in west Sikkim, from Khechipiri Lake [84] of the Late Holocene, showed that the moist climate persisted for around 2500 years (BC 500) and was more humid for around 1000 years (around AD 950), which covers the MWP. The pollen records from Jore–Pokhari Lake, Sikkim, and the Darjeeling Himalaya region adjacent to the present site demonstrate climate fluctuation for 2500 years [87]. A warm,

temperate, and humid climate prevailed in the region for around 2500 years BP (around BC 550), which is not observed in our climate reconstruction.

The short-term oscillation towards a cooler climate occurred between 1600 and 1000 years BP (AD 350–950),, which falls in DACP as observed in present reconstructions. The amelioration of climate that began between 1000 and 300 years BP (AD 950–1650) is related to MWP and transitions between MWP and LIA. At Paradise Lake in the eastern Himalayas, pollen-based records [165] show a warm and moist climate, similar to the prevailing present-day conditions around AD 240, which would represent the last part of the RWP. They also reported another such period that turned out to be warmer around 1100 cal years BP (AD 985), corresponding to the MWP. In this study at Paradise Lake, Bhattacharyya et al. [165] reported the impact of LIA in the eastern Himalayas on climate and vegetation fluctuations due to the cooler and less moist climate around AD 1400, after which it reverted to warm and moist conditions. The tree-ring-based temperature reconstruction from the adjoining Bhutan Himalaya [16] shows cold conditions during the early 15th, 16th, and late 17th to early 18th centuries. These cold periods fall within the LIA events recorded in our temperature reconstruction. The anomalous cold conditions observed in the Bhutan Himalayas are also reported in Europe [16,166] and central Asia [16,158,167,168], and these multidecadal to multicentennial cold timescales during the 15th to 18th centuries coincide with minima in solar energy output [16, 169, 170].

The MWP and LIA events and other past climate oscillations are also observed in the adjoining regions of the present study sites and other parts of the Himalayas. The pollen records from northeast India reported similar climate inferences. The inception of a relatively drier climate owing to a reduction in monsoon precipitation around 540 years BP onward (AD 1460) was reported as an LIA event in the lower Brahmaputra valley, northeast India [171]. From western Assam, northeast India experienced an increased warm and humid climate during 1950–989 cal years BP (AD 0–961), which has been reported to correspond to MWP [172]. The LIA event has existed since 989 cal years BP (AD 961) in western Assam, northeast India [172], which suggests that the cold period in this region started quite early in comparison with the present and other earlier studies. The adjacent Nepal Himalaya ice core records from Mt. Everest show a weakening summer monsoon influence since AD 1400, which may be associated with a reduction in solar irradiance and the onset of the LIA [173]. The cooler period is documented from AD 1605 to 1770 in Nepal using a network of 42 tree-ring chronologies from the whole of Nepal. The precipitation reconstruction using tree-ring data from the south-central Tibetan Plateau recorded the most extended wet period, which occurred in the first half of the 12th century, while the most prolonged dry phase started in the second half of the 16th century and lasted until the end of the 18th century [174].

Here, we also compared our climate reconstruction with pollen and other proxies-based studies carried out in other high-altitude regions of the Himalayas, Karakoram, and Pamir. The palaeoclimate record of the Late Holocene for 3500 years from the Pinder glacier, Kumaon Higher Himalayas [175] showed an abrupt rise in temperature as well as moisture at ~AD 400, after which the climate suddenly turned warm and moist and remained so until ~AD 1260, being referred to as the MWP. The record shows that the MWP period lasted much longer compared to present climate reconstructions. Based on the pollen analysis of a small number of samples from Tipra Bamak glacier [176], the authors believed the amelioration of climate around AD 1200 fell within the duration of the MWP. Furthermore, they recorded the deterioration of climate and glacier advancement around AD

1275–1408, which is considered to be within the time period of LIA. The vegetation vis–à–vis climate and glacial fluctuations of the Gangotri Glacier, Garhwal Himalaya showed the existence of a cooler climate between 2000 and 1700 years ago (BC 50–AD 250) [177]. This inference is comparable with another study in Ireland, where the same time period is a part of DACP [178]. In the Gangotri glacier between 1700 and 850 years ago (AD 250–1050), the climate witnessed amelioration. In Ireland, this time period was the transition phase from within the DACP to the midst of the MWP. Following this, 850 years ago (AD 1000), the climate in Gangotri region became much cooler, signifying its shift towards LIA conditions. Furthermore, 300 to 200 years ago (AD 1650–1750), the long-term retreat of the Gangotri glacier possibly ceased with some minor advancement. The pollen-based climatic record described by Kar et al. [177] from another large glacier of the western Himalayan region has past climatic fluctuations that resemble the ones at the present study site. The pollen-based records from Spiti, western Himalaya, identified past climate in relation to glacier advancement and retreat and the fluctuation of the tree line accordingly [179]. The glacier retreated and the tree line shifted to a higher elevation from 1500 to 900 cal years BP (AD 450–1050), and the glacier advanced and the tree line shifted to a lower elevation under a warm–moist climate (MWP). The region experienced cold–dry climate (LIA) from 900 cal years BP (AD 1050). Chauhan et al. [179] also recorded cold–dry climate from 2300 to 1500 cal years BP (BC 350–AD 450) comparable with the present study. However, another site located at a lower elevation also recorded the same three climatic events, but their initiation and termination duration are varied [179]. The pollen analysis from Parvati valley, western Himalaya [180], revealed the existence of two broad climatic episodes of warm–moist climate from AD 650 to 1200, equivalent to MWP, and cold–dry conditions from AD 1500 onwards that fall within the time period of LIA. The pollen records at Batal, in the vicinity of Rohtang Pass, western Himalaya [181] show climate amelioration during the period AD 1150–1450, which reverted to cold and dry conditions again after AD 1450, which might correspond to MWP and LIA, respectively. Pollen analysis supplemented with carbon isotope and total organic carbon from Chandra valley, Lahual, north-western Himalaya [182] reported climate amelioration, indicating a warm and moist climate corresponding to the MWP during the period ~1158 and 647 cal years BP (AD 792–1303). Furthermore, a cold–dry climate with weaker ISM intensity corresponding to LIA commenced between ~647 and ~341 cal years BP (AD 1303–1609) in the region. In addition to MWP and LIA events, Rawat et al. [182] also reported that the region witnessed a cool and moist climate with a relative weakening of the ISM during ~2032 and 1158 cal years BP (AD 82–792). This period of cool–moist climate was observed in the present study and also in western Himalaya [177,183]. In the western Himalayas, beside pollen records, elemental proxy records on sediment core from Badanital Lake, Garhwal Himalaya [184], describe the imprints of major global events such as the MWP, LIA, and modern warming. The MWP time period in their records prevailed around 920–440 cal years BP (AD 1030–1510). The spring temperature reconstructed using tree-ring data from the Garhwal Himalayas showed the most conspicuous feature of a long-term cooling trend since the late 17th century, which ended early in the 20th century [185]. The abrupt termination of this cooling is described as the end of the LIA. They also observed a warmer 30-year period in the latter part of the 17th century (AD 1662–1691). However, the long-term cooling trends in their records have a comparable LIA period to our present reconstruction. The dating of lichens from the Garhwal Himalayas reported various stages of the advances and retreat of the Chorabari glacier at a time when warming led to the demise of the LIA and the initiation of CWP and compared its similarity with findings from other parts of the globe [186]. In the central Indian Himalayas, the rapid growth rate of speleothem during AD 830–910 with higher precipitation, most likely the lower part of MWP, and the comparatively wetter environment spanning AD ~1440–1880 corresponding to the LIA time period,

were observed [187]. The moisture variations with respect to lake level fluctuation derived from lacustrine sediment of Sasikul Lake, Pamir Plateau, showed a pronounced wet period between AD 1550 and 1900, corresponding to the increase in LIA and lake level. The lowering of the lake level during AD 950–1200, described as MWP under dry climatic conditions [188]. Precipitation reconstruction over a millennium in the Karakoram Range using tree-ring $\delta^{18}O$ revealed a cluster of peak precipitation periods during the late 19th century [189]. The wet periods of decadal length occur around AD 1200, 1350, 1500, and 1870, and the dry periods occur before 1000 and around AD 1270, 1420, 1600, and 1720. This millennium reconstruction only showed punctuated wet and dry periods, but not long-term MWP or LIA-like events. However, a recent study showed that the temperature in Karakoram has been out of phase with the hemispheric trend for the past five centuries and did not record any cooling events in the LIA period [190].

It has been further observed that the widely researched climatic events MWP and LIA were also evident in the tropical belt and surrounding oceanic regions of India and comparable with present climate reconstruction. The pollen-based climate records of southeastern Madhya Pradesh, south India spanning the past 1650 years, identified three major climatic regimes and compared them with global climatic events [191]. The warm and moist climate with an increase in monsoon precipitation during AD 350–1250 corresponds with the period of the MWP. The period of less moist climate owing to the reduction in monsoon precipitation during AD 1250–1650 is described as LIA. The last phase was a warm period that has now persisted for three centuries. The adjoining region, i.e., southwestern Madhya Pradesh, central India, also witnessed a warm and moderately humid climate during 1416–506 cal years BP (AD 534–1444) based on pollen records [192], and a warm and humid climate since AD 1444, which they considered LIA. Signs of the LIA period for 1300 years BP (AD 650) with a relatively dry climate have been reported from western Odisha in eastern coastal India [193]. Besides pollen, the cave records from central India revealed the existence of the MWP between about AD 920 and 1340 and mentioned a much wetter regime than the subsequent LIA [194].

The record from the northeastern Arabian Sea using organic C and N concentrations [195] showed that the intensity of the Indian monsoon decreased during the LIA but increased during the MWP (~ AD 1050–1300). Similarly, the planktic foraminifer study carried out in the northwestern Arabian Sea [196] indicated that southwest monsoon winds were stronger during the MWP (AD 800–1300) and coincident with a period of high solar activity. The monsoon winds reconstruction using foraminifera data of *Globigerina bulloides* from Arabian Sea box cores indicates increasing monsoon winds since AD 1600 [197]. A humid climate and enhanced precipitation during the terminal stages of the LIA have also been observed using oxygen isotope data from foraminifera from the southeastern Arabian Sea [198]. An oscillating precipitation was recorded in varve chronology from the northeastern Arabian Sea [199]. These records showed precipitation minima during BC 250–AD 50 and around AD 950, and the authors considered these precipitation minima to correspond to RWP and the initiation of MWP as well as increasing varve thickness since AD 1400, suggesting increasing precipitation.

Thus, we can infer that the pollen-based records from the eastern Himalayas [84,85,87,165], western Himalayas [175-177,179,180-182], northeast India [171,172], central India [191,192], and east coastal India [193] described signals of the widely researched and debatable climatic events MWP and LIA, similar to the present study, which shows how vegetation vis–à–vis the climate responded to global climate change. Besides pollen, other proxy records such as ice core [173]; elemental analysis

[184]; Lichen dating [186]; and tree-ring from the western Himalayas [185], Nepal [200], Karakoram [189], Tibetan Plateau [174], and Bhutan Himalaya [16]; speleothem from the central Indian Himalayas [187]; stalagmite records from central India [194]; varve chronology and organic C and N concentration from the north eastern Arabian Sea [195,199]; Foraminifera records in the northeastern Arabian Sea [196,198]; and lake level fluctuation using lacustrine sediments from the Pamir plateau [188] identified climatic fluctuations during the MWP and LIA.

The comparative climatic events, especially MWP and LIA, in these records from various geographical regions within the present climate reconstruction showed that the dates of initiation and termination of both MWP and LIA are not coeval (Figure 10). Thus, the difference in the time interval of the MWP and LIA events observed in the present climate reconstructions in comparison with other records from India and adjoining Indian regions is reasonable. In general, it is believed that the climatic events of the MWP and LIA are warm (humid) and cold (dry), respectively. However, this is not homogenous for all studies (Figure 11). Qualitative comparative studies carried out showed differences in climatic inference in a few records [172,188,192,197-199]. The study on hydroclimatic changes in China and its surrounding regions during the MCA (MWP) and LIA, with special emphasis on its spatial patterns and possible mechanisms, reviewed 71 proxy records [201]. They conserved the periods of MCA/MWP and LIA as AD 1000–1300 and AD 1400–1900, respectively, and showed the variability of the occurrence of wet, moderate, and dry episodes in each of the 71 sites. The moisture variations during MCA/MWP, and LIA are influenced by sea surface temperature and atmospheric modes from region to region [201]. Thus, differences in climate episodes such as moist and dry from site to site during the MWP and LIA periods are reasonable in different parts of Asia, including India and adjoining regions. The model data and ensemble simulation comparison for the last millennium of climate variability also discussed the role of internal and forced responses, which concluded that differences in climate during the MWP and LIA between different locations are likely [202]. However, even with differences in duration and climatic conditions during MWP and LIA, the findings from the various parts of the Himalayas and adjoining areas showed consistency with our climate reconstruction from the Zemu glacier, eastern Himalayas (Figure 10). Our study showed the presence of MWP and LIA with warm–moist and cold–dry climatic conditions at the present study sites (Figure 11).

In the present climate reconstruction, it has been noticed that the characteristic cold and dry environments have returned to warm and moist conditions since the middle to late 19th century and again returned to cold, dry conditions (Figure 8). This could be due to the persistence of intensified atmospheric circulation. Similarly, a change in monsoonal circulation since 1400 AD was also observed in the adjoining region of Nepal [173]. This suggests that LIA atmospheric conditions continued during the early 20th century despite the warming during the middle to late 19th century that is commonly regarded as the end of the LIA. A similar observation is reported in [173,203,204]. In the south-central Tibetan Plateau, tree-ring data showed an increasing precipitation trend from the second half of the 20th century to the present day. The reconstruction indicates unprecedented pluvial conditions for the past decade [174].